









## ORIGINAL ARTICLE

# Expression patterns of melanin-related genes are linked to crypsis and conspicuousness in a pumpkin toadlet

Juliane P. C. Monteiro<sup>1,2,3,4</sup>  | Heike Pröhl<sup>4</sup>  | Mariana L. Lyra<sup>3,5</sup>  |  
 Andrés E. Brunetti<sup>3,6,7</sup>  | Eli C. de Nardin<sup>2</sup>  | Thais H. Condez<sup>3,8</sup>  |  
 Célio F. B. Haddad<sup>2,3</sup>  | Ariel Rodríguez<sup>4</sup> 

<sup>1</sup>Post-Graduate Program in Biodiversity, Institute of Biosciences, São Paulo State University (UNESP), Rio Claro, São Paulo, Brazil

<sup>2</sup>Department of Biodiversity and Aquaculture Center (CAUNESP), Institute of Biosciences, São Paulo State University (UNESP), Rio Claro, São Paulo, Brazil

<sup>3</sup>Center for Research on Biodiversity Dynamics and Climate Change, Institute of Biosciences, São Paulo State University (UNESP), Rio Claro, São Paulo, Brazil

<sup>4</sup>Institute of Zoology, University of Veterinary Medicine of Hannover, Hannover, Lower Saxony, Germany

<sup>5</sup>New York University Abu Dhabi, Abu Dhabi, United Arab Emirates

<sup>6</sup>Institute of Subtropical Biology (IBS, UNaM-CONICET), Posadas, Misiones, Argentina

<sup>7</sup>Department of Insect Symbiosis, Max Planck Institute of Chemical Ecology, Jena, Thuringia, Germany

<sup>8</sup>Department of Earth Sciences, Carleton University, Ottawa, Ontario, Canada

## Correspondence

Juliane P. C. Monteiro, Department of Biodiversity and Aquaculture Center, Institute of Biosciences, São Paulo State University (UNESP), Rio Claro, São Paulo 13506-900, Brazil.

Email: [julianepmonteiro@gmail.com](mailto:julianepmonteiro@gmail.com)

Ariel Rodríguez, Institute of Zoology, University of Veterinary Medicine of Hannover, Hannover, Lower Saxony 30559, Germany.

Email: [ariel.rodriguez@tiho-hannover.de](mailto:ariel.rodriguez@tiho-hannover.de)

## Funding information

Conselho Nacional de Desenvolvimento Científico e Tecnológico, Grant/Award Number: 163546/2020-7 and 306623/2018; Deutsche Forschungsgemeinschaft, Grant/Award Number: RO5508/2-1; Consejo Nacional de Investigaciones Científicas y Técnicas, Grant/Award Number: PIP/2021-2023; Fondo para la Investigación Científica y Tecnológica, Grant/Award Number: 2020/2939; Fundação de Amparo à Pesquisa do Estado de São Paulo, Grant/Award Number: 2018/09691-0, 2021/08799-4 and 2021/10639-5; Deutsche Gesellschaft für Herpetologie und Terrarienkunde, Grant/Award Number: WP-01/2022

Handling Editor: Sarah Perry Flanagan

## Abstract

Colour signals play pivotal roles in different communication systems, and the evolution of these characters has been associated with behavioural ecology, integumentary production processes and perceptual mechanisms of the species involved. Here, we present the first insight into the molecular and histological basis of skin colour polymorphism within a miniaturized species of pumpkin toadlet, potentially representing the lowest size threshold for colour polytypism in tetrapods. *Brachycephalus actaeus* exhibits a coloration ranging from cryptic green to conspicuous orange skin, and our findings suggest that colour morphs differ in their capability to be detected by potential predators. We also found that the distribution and abundance of chromatophores are variable in the different colour morphs. The expression pattern of coloration related genes was predominantly associated with melanin synthesis (including *dct*, *edn1*, *mlana*, *oca2*, *pmel*, *slc24a5*, *tyrp1* and *wnt9a*). Up-regulation of melanin genes in grey, green and brown skin was associated with higher melanophore abundance than in orange skin, where xanthophores predominate. Our findings provide a significant foundation for comparing and understanding the diverse pathways that contribute to the evolution of pigment production in the skin of amphibians.

## KEYWORDS

Anura, *Brachycephalus*, colour polymorphism, gene expression, skin chromatophores, visual modelling

This is an open access article under the terms of the [Creative Commons Attribution-NonCommercial-NoDerivs](https://creativecommons.org/licenses/by-nc-nd/4.0/) License, which permits use and distribution in any medium, provided the original work is properly cited, the use is non-commercial and no modifications or adaptations are made.

© 2024 The Author(s). *Molecular Ecology* published by John Wiley & Sons Ltd.

## 1 | INTRODUCTION

Coloration in animals is involved in different evolutionary functions related to physical protection (e.g. thermoregulation and UV protection), inter- and intra-specific signalling (e.g. sexual and social selection) and/or as a strategy to avoid predation (e.g. camouflage, mimicry or aposematism) (Hutton et al., 2015; Rojas, 2017; Ruxton et al., 2018). Colour is a physical phenomenon and emerges from the intricate interplay between the reflection of light from the skin, scales, feathers or hairs of the bearer, as well as the sensory receptors and the cognitive architecture of the observer (Maia et al., 2019; Osorio & Vorobyev, 2008; Renoult et al., 2017). Understanding the diversity of colour phenotypes provides valuable insights into the adaptive significance of coloration and the complex mechanisms driving biodiversity in the natural world (Briolat et al., 2019; Caro, 2017; Emberts & Wiens, 2022; Stuart-Fox et al., 2021). However, while ecological functions of coloration in animals have been studied for over a century (Caro, 2017; Müller, 1879), the molecular and structural bases of colour determination are less known (Hashimoto et al., 2021; Shawkey & D'Alba, 2017).

Amphibians are one of the most diverse classes of vertebrates, with an extraordinary diversity of colours at inter- and intra-specific levels (Rojas, 2017), though this diversity has been addressed only recently and for a few species' groups (Rojas, 2017). Within anurans, studies of colour variation were centred on poison frogs (Anura: Dendrobatidae), which exhibit classical colour variability within species, from colour polymorphism (within populations) to polytypism (between populations) (e.g. Brusa et al., 2013; Rojas et al., 2018; Twomey, Johnson, et al., 2020). Studies employing genomic approaches showed that colour variation in poison frogs is controlled by multiple genes (Rodríguez et al., 2020; Stuckert et al., 2019). In addition, they demonstrated that various pathways, like carotenoid processing (Rodríguez et al., 2020; Twomey, Johnson, et al., 2020), melanin synthesis (Posso-Terranova & Andrés, 2017; Stuckert et al., 2019), pteridine synthesis (Rodríguez et al., 2020) as well as the genes involved in structural coloration and pigment cell development (Stuckert et al., 2019), have a significant contribution to skin colour variation. Nevertheless, similar phenotypes in closely related species may exhibit divergent mechanisms of colour production (Twomey et al., 2023).

Concerning the structural bases of colour variation, amphibians attain this variability by combining complex structural and pigimentary cell components. Bagnara et al. (1968) identified three cell components as the main ones responsible for amphibian coloration and defined it as the 'dermal chromatophore unit'. In this arrangement, the layer closest to the epidermis consists of xanthophores containing carotenoid and pteridine pigments reflecting from yellow to red hues. The middle layer comprises iridophores containing reflective purine (e.g. guanine) crystal platelets that contribute to structural colours. The deepest layer consists of melanophores, which have melanosomes with melanin pigments absorbing light across a broad spectrum, producing dark colours (Andrade & Carneiro, 2021; McNamara et al., 2021; Shawkey & D'Alba, 2017). However, this

cellular structural arrangement is not observed in several species, like those with vibrant green colours lacking melanophores (Taboada et al., 2020). Colour differences among body regions within the same individual can also be explained by the presence of only xanthophores and/or iridophores (Frost & Robinson, 1984; Kindermann & Hero, 2016) or pigment variation within xanthophores and platelets morphology in iridophores (e.g. Twomey, Johnson, et al., 2020; Twomey, Kain, et al., 2020). Although the link between genetic and morphological data might seem obvious, studies correlating these two sources of evidence are scarce (Posso-Terranova & Andrés, 2017).

Recent advances in genomics have enabled several investigations of evolutionary mechanisms associated with genotype-phenotype interaction in non-model species (Andrade et al., 2022; Goutte et al., 2022; San-Jose & Roulin, 2017). The direct-developed species of the genus *Brachycephalus* (Anura: Brachycephalidae) are miniaturized amphibians with ground-dwelling and diurnal activity, endemic to the Brazilian Atlantic Forest (dos Reis et al., 2020). Species in this genus have a wide range of skin colour variation, from bright yellow/orange (the pumpkin toadlets,  $N=36$ ) to dark brown species (the flea toads,  $N=5$ ) (Condez et al., 2020; Frost, 2024; Lyra et al., 2021). The evolution of bright coloration in pumpkin toadlets seems to be related to body plan (bufoniform) and the presence of tetrodotoxin, a potent neurotoxin (Chimetto Tonon et al., 2021; Hanifin, 2010; Pires et al., 2005). Because of this colour-toxin association, pumpkin toadlets are assumed to have aposematic antipredator strategies, though experimental evidence testing this inference is rare (Rebouças et al., 2019).

The pumpkin toadlet *Brachycephalus actaeus* has a restricted and relatively small distribution range of approximately 80 km<sup>2</sup>, inhabiting pristine forests in the northeastern Brazilian state of Santa Catarina (Monteiro et al., 2018). The populations of this species present intriguing colour polytypism (Lyra et al., 2021; Monteiro et al., 2018), with at least four distinct colour morphs: brown, grey, green and orange (Monteiro, J.P.C. pers. obs.). It is the unique species in the genus known to have such intra-specific colour variation. By using a population dataset from this species, we first tested if a potential bird predator can perceive the distinct colour morphs of *B. actaeus*. Second, we characterized the skin histology from the different colour morphs. Finally, we used comparative transcriptomic analyses from the skin to identify candidate coloration related genes in the different colour morphs. Our results represent the first step to understanding colour polytypism in *Brachycephalus*. They significantly contribute to testing hypotheses regarding colour divergence, its ecological significance and the underlying molecular mechanisms in amphibians.

## 2 | MATERIALS AND METHODS

### 2.1 | Field sampling and procedures

We conducted fieldwork from 01 to 08 October 2021 at six geographic localities across the known distribution range of *B. actaeus*

in the northeastern state of Santa Catarina, Brazil. We sampled at least five individuals per locality, totalling 39 collected specimens covering all colour morphs (Table S1). The localities belong to the municipalities of Itapoá (Alto Braço do Norte [BNb; brown morph] and Baixo Braço do Norte [BNg; green morph]) and São Francisco do Sul, at the mainland of Distrito do Saí (Casarão [CAS; grey morph]; Morro do Cantagalo [CAG; orange morph] and Vila da Glória [GLO; green morph]) and at São Francisco do Sul Island (Serra da Palha [SPA; green morph]). At all sampling localities, the air humidity was around 90%–100% and the temperature range was 18–22°C.

The collected specimens were euthanized by cutaneous anaesthetic overdose (5% lidocaine). Immediately afterwards, we skinned the specimens, resected them and divided the skin into sagittal halves. One-half of the skin was stored in RNAlater for RNA-Seq analyses at –80°C until the RNA extraction and the other half was used in histological analyses (see next). All samples were collected in compliance with the Ethics Committee of the São Paulo State University, Rio Claro, São Paulo, Brazil (UNESP; protocols #02/19), under the research permit issued by the Sistema de Autorização e Informação em Biodiversidade from the Instituto Chico Mendes de Conservação da Biodiversidade – Ministério do Meio Ambiente, Brazil (SISBIO #63104-4). We also registered access to genetic information on the National System for the Management of Genetic Heritage and Associated Traditional Knowledge (SISGen #A91405E). Voucher specimens were deposited in the Célio F. B. Haddad (CFBH) Amphibian Collection, housed at the Departamento de Biodiversidade, Instituto de Biociências, UNESP, Rio Claro, São Paulo, Brazil.

## 2.2 | Colour morph classification and bird visual modelling

To classify *B. actaeus* individuals according to colour morph, we first tested whether they could be perceived by potential predators as four distinct colours in the same way as we do. While specific predators of *B. actaeus* and also from other *Brachycephalus* species remain unknown, there is a rare record of a tinamou bird (Palaeognathae: Tinamidae, *Tinamus solitarius*) preying on *Brachycephalus ephippium* (Carvalho, 1940), and an experimental test of *Brachycephalus*' aposematic role under chicken predation (Rebouças et al., 2019). Considering that and given that birds are considered significant predators of Neotropical poison frogs (Casas-Cardona et al., 2018; Dreher et al., 2015; Willink et al., 2014), we choose the visual system of the peafowl (Neognathae: Phasianidae, *Pavo cristatus*), a ground feeder bird, as a model for testing the perception of a potential predator. Galliforms (peafowl and chicken) and tinamou birds lack ultraviolet sensitivity (Wright & Bowmaker, 2001) and were assumed to represent the best available model for our dataset.

Briefly, we captured RAW format images of the 39 toadlets and the natural backgrounds using neutral reflectance grayscale within the human visible spectrum (400–700nm). The camera's sensitivity in the red, blue and green (RGB) channels was determined and calibrated to generate a cone catch model for the visual system of

the peafowl under daylight D65 illuminant. Next, multispectral images (mspec) were created from toadlets and backgrounds. Finally, we obtained the photon catches from short-wave-sensitive (SWS; blue), medium-wave-sensitive (MWS; green), long-wave sensitive (LWS; red) and double cones (DC) receptors in the bird's retina. We used micaToolbox version 2.2.2 (Troschianko & Stevens, 2015) in ImageJ version 1.52k (Schneider et al., 2012) for all steps of image calibration.

For colour morph classification, we utilized the peafowl photon catch sensitivities from both dorsal and lateral images of *B. actaeus* individuals (eight variables; see Appendix S1). These data were employed to investigate overall variation and categorize individuals into discrete colour morph categories. Three non-correlated variables (Pearson's  $r > 0.7$ ), SWS and MWS from lateral and LWS from dorsal images were used as input for Gaussian mixture modelling using mclust version 6.0.0 (Fraley et al., 2012) in R version 4.1.2 (R Core Team, 2021). Multiple models were run with  $k = 1$ –10 clusters in the data and 999 bootstrap replicates, combining the data's orientation, volume and shape (Fraley et al., 2012). The best-fit model was determined using the Bayesian information criterion (BIC). Finally, we performed the receptor noise-limited bird visual model (Vorobyev & Osorio, 1998) to quantify and compare perceptual differences among *B. actaeus* morphs.

Appendix S1 provides detailed information on macro photography procedures, camera calibration, image processing and visual modelling.

## 2.3 | Structural and ultrastructural analyses of the skin

The dorsal and ventral skin of *B. actaeus* from 12 individuals (two individuals per locality) were processed and examined (Table S1). Detailed methods of skin preparation are given in the Appendix S1. To analyse the skin structure, preparations of semi-thin (for light microscopy, LM) and ultrathin (for transmission electron microscopy, TEM) sections were performed at the Multiuser Laboratory of Electronic Microscopy of the University of São Paulo (Faculdade de Medicina de Ribeirão Preto, Ribeirão Preto, São Paulo, Brazil). The semi-thin preparations were examined under an Olympus BX51 light microscope coupled to a DP71 digital camera using a magnifying strength of 60× and 100× to capture images with a resolution of 432 dpi. The ultrathin sections were observed with a JEOL JEM 100CXII transmission electron microscope at 80kV acceleration voltage. Contrast and brightness were adjusted using the equipment software.

We used LM images to describe the skin layers (i.e. epidermis, dermal *stratum spongiosum* and *compactum* and calcified layer) following Brunetti et al. (2016) and Toledo and Jared (1993). We measured the thickness of layers using the image analysis in Fiji version 2.9.0 (Schindelin et al., 2012). To obtain the average skin thickness, we took three calibrated measurements per layer (anterior, medial and posterior sections) for each sample, measuring two replicates per sample.

We used LM and TEM images to characterize chromatophores. We followed Bagnara et al. (1968) and Frost and Robinson (1984) to identify intracellular pterinosome and carotenoid vesicles and melanosomes from xanthophores and melanophores respectively. We quantified the chromatophores of semi-thin samples using the Trainable Weka Segmentation plugin version 3.0 (Weka; Arganda-Carreras et al., 2017) in Fiji version 2.9.0 (Schindelin et al., 2012). First, we manually picked the chromatophore layer to measure the total area. Next, we trained the algorithm using Weka, selecting similar pixels corresponding to the attributes background, melanosome and xanthophore, including a minimum of 20 ROI sets for each class. Finally, we created a mask to measure the coverage of the melanosomes and xanthophores based on image segmentation results. We considered the area covered by melanosomes or xanthophores divided by the total area of the chromatophore layer in each colour morph (Figure S1).

## 2.4 | RNA sequencing, reference transcriptome assembly and annotation

RNA extraction from the skin (sagittal half) and library preparation were performed by Genewiz® (Leipzig, Germany) with PolyA selection using Illumina® NovaSeq™ sequencing system for 26 individuals of *B. actaeus* (four to five individuals per locality; Table S1). Samples were then prepared using the Illumina® stranded Tru-Seq® library protocol and pair-end sequenced with 150bp reads in an Illumina® NovaSeq platform. The methodology employed for constructing the reference transcriptome followed these steps: (i) conducting quality check and pre-processing of raw reads, (ii) performing de novo transcriptome assembler, (iii) generating non-redundant transcript data and evaluating transcriptome assembly and (iv) annotation of a reference transcriptome.

We performed a quality control of sequencing stats per sample using FastQC version 0.12.1 (Andrews, 2010). We then used Trimmomatic version 0.32 (Bolger et al., 2014) to remove adapters and low-quality fragments before pooling the samples per locality. Reads were then concatenated by locality, normalized to a target depth of 50x using bbnorm version 38.08 (Bushnell, 2014) and rRNA decontaminated with SortMeRNA version 2.0, using contaminant database version 4.3 (Kopylova et al., 2012). To minimize variant-derived assembly artefacts, we opted for a stratified consensus approach in which we performed a de novo transcriptome assembly from the pool of sequencing reads per locality before constructing a consensus transcriptome assembly for the species. Then, we used three different de novo transcriptome assembly algorithms using their default setting unless specified to assemble the read collections per locality: Trinity version 2.14.0 (--SS\_lib\_type RF and --min\_kmer\_cov 2 options) (Haas et al., 2013); rnaSPADES version 3.9 (--ss rf) (Bushmanova et al., 2019) and SOAPdenovo-Trans version 1.03 (executed four times, with  $k$ -mers=19, 37, 55 and 73, max read length=150, average insert size=400 and nasm\_flag=3) (Xie et al., 2014). The resulting 36 assemblies (6x Trinity,

6x rnaSPADES and 24x SOAPdenovo-Trans) were combined into a comprehensive reference transcriptome using EvidentialGene version 4 (Gilbert, 2019), which filters the collection of transcripts by selecting the most extended coding sequence and related isoforms while removing redundant sequences. We evaluated transcriptome completeness by their BUSCO scores against the 3354 vertebrate benchmarking genes in the vertebrate odb\_database version 10 (Simão et al., 2015).

The resulting reference transcriptome was annotated using EnTap pipeline version 0.10.9 (Hart et al., 2020). The pipeline was configured with Transdecoder (<https://github.com/TransDecoder>) for open reading frame (ORF) detection, RefSeq Vertebrates (<https://www.ncbi.nlm.nih.gov/refseq/>; accessed on June 2022), UniProt (The UniProt Consortium, 2019; accessed on June 2022) protein databases for similarity searches with Diamond version 0.9.22 (Buchfink et al., 2014) and EggNOG version 5 database (Huerta-Cepas et al., 2019; accessed on March 2022) for orthology searches. Blast hits on bacteria, fungi, nematodes and viruses were flagged as contaminants and excluded. The final annotation of protein names used the results of reciprocal best blast hits (E-value:  $1e-5$ ) against *Xenopus tropicalis* proteome complemented with UniProt protein database hits obtained from EnTap.

## 2.5 | Population structure

We used Lace software version 3.17 (Davidson et al., 2017) to concatenate the transcripts in the reference transcriptome into a set of super-transcripts, each containing all exon sequences of a given gene concatenated without redundancy. A gene-to-transcript map was obtained with Corset version 1.09 (Davidson & Oshlack, 2014) and was used as input to Lace to guide the concatenation of transcripts. The resulting super transcriptome was used as a reference against which all RNA-Seq reads were mapped using STAR version 1.1.13 (Dobin et al., 2013). Variants were called using GATK software version 1.8 (McKenna et al., 2010), following the best-practice workflow for RNA-Seq SNP calling (Van der Auwera & O'Connor, 2020). This pipeline includes aligning, sorting and marking duplicate read mappings, split reads into exon segments and clip sequences overhanging the intronic regions (SplitNCigarReads). Variants were called with phred-scaled confidence threshold >20 and later filtered to retain those with Fisher strand values (FS) >30.0 and quality-by-depth values (QD) <2.0. The resulting VCF file was further filtered using vcftools (Danecek et al., 2011) to include only bi-allelic SNPs, with a minor allele frequency >0.04 (more than two allele copies in 26 diploid individuals) and <50% missing data across individuals.

The SNP dataset was pruned to remove variants in linkage disequilibrium, as estimated by the correlation of genotypes using the '--indep-pairwise 50 5 0.2' options in PLINK version 1.9 (Purcell et al., 2007). We then used the resulting genotypes to ascertain population structure by running 20 repetitions of ADMIXTURE version 1.3 (Alexander et al., 2009) for  $K=1-10$ . A principal component

analysis (PCA) inspection was performed using PLINK version 1.9 (Purcell et al., 2007) and the results were visualized using the R package tidyverse version 2.0.0 (Wickham et al., 2019).

## 2.6 | Differential gene expression analyses

Transcript abundance in the skin samples was estimated by pseudo-aligning the quality-trimmed reads to the EvidentialGene reference transcriptome with Kallisto software version 2.8.12 (Bray et al., 2016) using 100 bootstraps for uncertainty estimation.

Differential expression analyses were then conducted with the 3DRNASeq package version 2.0.1 (Guo et al., 2021). We imported Kallisto transcript abundance estimates, normalizing them by transcript per million (TPM). We summarized these at the transcript and gene levels using the gene-to-transcripts mapping output from EvidentialGene. We retained transcripts occurring in  $\geq 4$  samples and showing  $\geq 1$  CPM. Then, we inspected the data, plotting a PCA of gene expression by sample. After filtering, expression estimates were normalized using the trimmed mean of  $M$  values (TMM) between-sample normalization. We performed statistical tests to identify differentially expressed genes (DEGs) in pairwise colour morph contrasts, one-versus-all contrasts between colours, and (orange + brown) versus (green + grey) groups. Statistical tests were conducted using the limma-voom analysis (Ritchie et al., 2015). A Benjamini–Hochberg procedure for error rate correction was applied before evaluating statistical significance with an  $\alpha=0.05$  and a log2 fold change of 1.

We focused on coloration related genes since we were interested in colour morph variation. To identify them, we compiled a list of genes linked in the melanin synthesis pathway, carotenoid metabolism, pteridine synthesis, iridophore guanine synthesis (Braasch et al., 2007; Higdon et al., 2013; McLean et al., 2017) and other pigmentation associated genes with diverse functions (Baxter et al., 2019) (Table S2). This list is undoubtedly not exhaustive, as the molecular mechanisms of colour production in amphibians, particularly in these toadlets, are poorly known. For gene nomenclature, we followed Xenbase version 6.0.0 (Fisher et al., 2023).

We compared our list of DEGs with those detected among colour phenotypes in three other dendrobatids *Dendrobates auratus* (Stuckert et al., 2019), *Oophaga pumilio* (Rodríguez et al., 2020) and *Ranitomeya sirensis* (Twomey, Johnson, et al., 2020; Twomey, Kain, et al., 2020).

## 2.7 | Transcriptome-wide association analysis

Classical differential gene expression tests typically compare samples grouped into categorical conditions. However, the statistical literature suggests that using continuous predictors in regression-like analyses often outperforms the categorical based ones in power, parsimony and interpretability of results (Lazic, 2008). Few existing

methods are both effective and computationally efficient for gene expression data (Sofer et al., 2021; van Rooij et al., 2019). While colour phenotypes can be categorized, as we did with our 3DRNASeq analysis, the variation among individuals is inherently continuous by nature. Therefore, analysing gene expression in relation to continuous coloration variables enhances statistical power and allows for the inclusion of covariates to control for genetic structure and other confounding factors. The combinations of analyses using both categorical and continuous predictors can provide complementary insights into gene expression patterns.

We used the chromatic discriminability in units of just noticeable differences of the toadlets from bird perceptual space to access visual perceptual distances (from the *jnd2xyz* function output in *pavo2* version 2.7.1, see Appendix S1; Maia et al., 2019; Pike, 2012). The y-coordinate of perceptual space scores was strongly correlated with the x-coordinate values, and only the uncorrelated x-axis and luminance scores were included in this analysis. We implemented a linear regression model that correlates changes in the TPM normalized expression values aggregated at the gene level (as obtained with Kallisto and 3DRNASeq, see before) with x-axis and luminance scores to test for gene expression association using *Olivia* package version 0.1.0 (Sofer et al., 2021). We filtered out low-expressed genes by removing those with more than 25% of samples with zero counts, maximum expression  $>5$  and maximum expression  $<10$ . Zero values were replaced with half the minimum non-zero values in the sample and the expression values were log2 transformed ('log\_replace\_half\_min' transformation). Subsequently, we fit the linear regression model to the transformed expression values, incorporating population structure as a covariate in the model (represented by the averaged admixture proportions obtained for  $K=2$  in the admixture runs). To evaluate the statistical significance of our results, we ran 100 residual permutations, considering them as associated in expression with the perceptual space coordinates of those genes with false detection rate (FDR) with  $p$  values  $<0.05$ .

## 2.8 | Gene co-expression network analyses

Correlations in the expression profile of multiple genes across samples can be represented by gene–gene interaction networks. We used the normalized expression values from 3DRNASeq (already excluding lowly expressed genes) as input for a weighted gene co-expression network analysis using the WGCNA package (Langfelder & Horvath, 2008) in R. We selected appropriate soft-thresholding power for network construction (12 in our case) by inspecting the mean connectivity/scale independence versus soft-threshold power plots. A signed network adjacency was then calculated from the expression data using Pearson's correlation and the selected soft-threshold power and translated into topological overlap measure (TOM) dissimilarities. Genes were then clustered into a dendrogram based on their TOM dissimilarity and gene modules were defined by applying a dynamic tree cut with



a minimum module size ( $\text{minClusterSize}=30$ ) and a medium sensitivity to branch splitting ( $\text{deepSplit}=2$ ). We then computed the eigengene values per module (i.e. the scores on the first principal component of expression) and correlated these with the two continuous uncorrelated toadlets' colour variables (x-coordinate and luminance in bird perceptual space, see section earlier) using Pearson's correlation ( $\alpha=0.05$ ). An overall description of the genes included in those colour-associated modules was obtained via an overrepresentation analysis of Gene Ontology terms in PANTHER version 18.0 (Thomas et al., 2022) using the *Homo sapiens* database at the biological process level and with FDR correction for multiple testing.

### 3 | RESULTS

#### 3.1 | Colour classification and bird visual modelling

According to the modelled peafowl perception of the spectral reflectance values, the mclust algorithm classified the individuals of *B. actaeus* into four clusters ( $\text{BIC}=573.7876$ ; Table S2). The classification error of the best-fitting Gaussian multivariate model (mixture of ellipsoidal, varying volume, shape and orientation coded as VVV

in Figure S2) was 0.04. The composition of these clusters matched the categorization into colour morphs by a human observer (JPCM; Table S3) with a 0.15 error. We hereafter refer to these morphotypes as brown, grey, green and orange morphs.

The toadlet-to-background contrasts for peafowl showed in the dorsal view that orange (CAG) and grey (CAS) colour morphs were the most distinctive in both colour contrast ( $\Delta S$ ) and brightness contrast ( $\Delta L$ ) values, while the green and brown morphs clustered together. In lateral view, however, the orange and brown morphs were distinct from the green and grey morphs, with this differentiation being more evident in  $\Delta S$  values (Figures 1 and Figure S3). In summary, the orange morph is the most conspicuous phenotype in dorsal and lateral coloration. The brown morph is conspicuous only when viewed laterally, where orange colour is present. The green and grey morphs are the least contrasting against the background, both in dorsal and lateral views.

#### 3.2 | Skin characterization

Overall, two distinct dermal regions (i.e. *stratum spongiosum* and *stratum compactum*) were easily recognized in the skin of *B. actaeus*, which are separated by a thickened calcified Eberth-Kastschenko

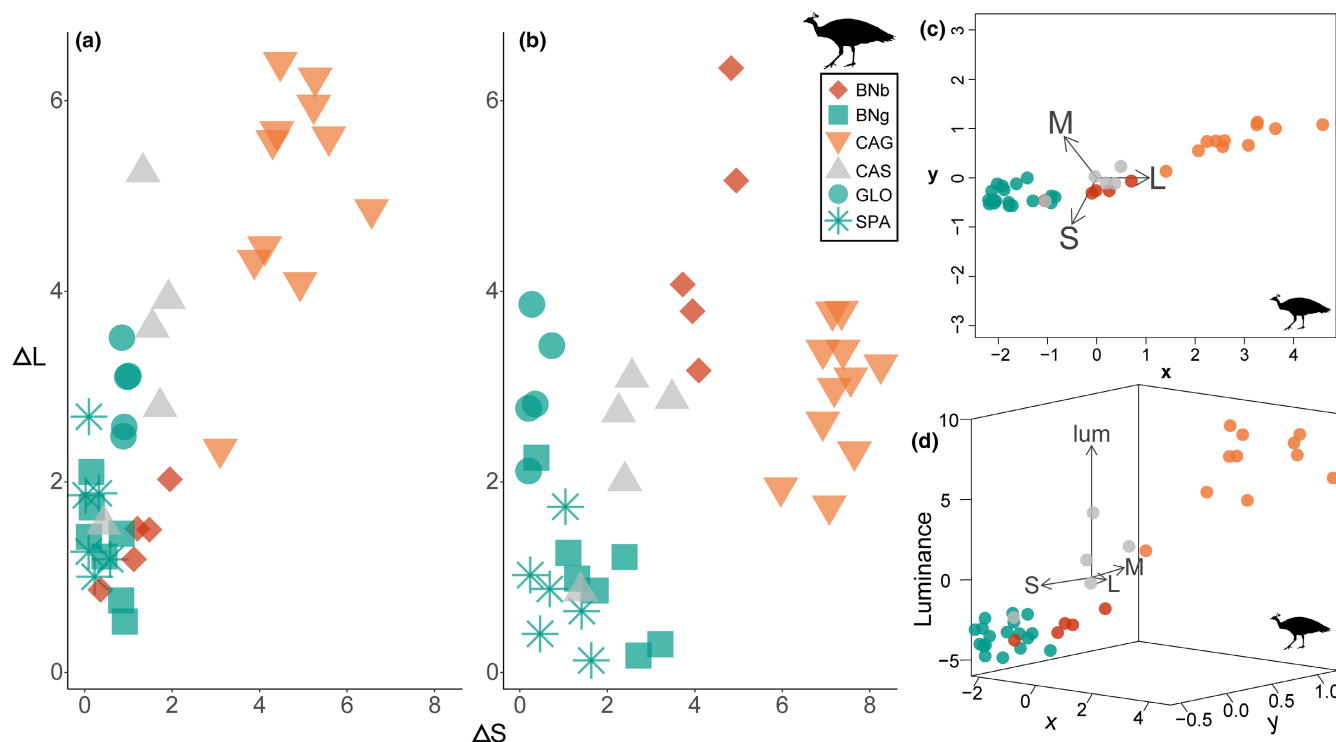


**FIGURE 1** Plots show the position of individuals in the perceptual space of predatory bird (peafowl). Colour ( $\Delta S$ ) and brightness ( $\Delta L$ ) visual contrasts of *Brachycephalus actaeus* individuals from the six study sites in dorsal (a) and lateral (b) views. The averages of inter-individual scores from colour and brightness contrasts were projected into x and y coordinates representing the average perceptual space (c) and their positions into x, y and luminance coordinates in a tetrahedral model of bird vision (d). Loadings of the original quantum catch variables are represented with dark grey arrows. Individuals are coloured by their colour morphs. Contrasts were calculated for each toadlet against the original background, assuming natural light conditions. BNb, Alto Braço do Norte; BNg, Baixo Braço do Norte; CAG, Cantagalo; CAS, Casarão; GLO, Vila da Glória; and SPA, Serra da Palha. Colours represent morphs identified (brown [BNb], grey [CAS], green [BNg, GLO, SPA] and orange [CAG]).

(EK) (Figure 2, Figure S4 and S5; Table 1 and Table S4). Only two types of chromatophores (melanophores and xanthophores) were identified in the *stratum spongiosum* of dorsal and ventral skin, with no iridophores recognized in any sample. The distribution and abundance of melanophores and xanthophores vary among morphs and between dorsal and ventral skin (Figure 2 and Figure S5; Table 1 and Table S4).

In the dorsal skin of orange toadlets, melanophores were either absent or very scarce, while xanthophores were abundant containing carotenoid vesicles and pterinosomes (Figure 2a,b; Table 1). In the brown and grey toadlets, the melanophores and xanthophores occurred similarly, with melanophores located either below or mingled with xanthophores (Figure 2c–f). Meanwhile, in the green

toadlets, the melanophores were more abundant, whereas xanthophores were much rarer (Figure 2g,h). Unlike the orange morph, xanthophores of grey, brown and green morphs only have pterinosomes but no carotenoid vesicles (Figure 2b,d,fh).

In the ventral skin of green morphs, the melanophores occurred in clusters and the xanthophores were more abundant than in the dorsal region. This pattern can be linked to the orange skin with dark blotches observed externally (Figure S5j–l; Table 1). In contrast, the very scarce presence of melanophores in the grey morph or their absence in the ventral skin of brown and orange morphs supports the occurrence of homogeneous orange bellies observed externally (Figure S5a–i). Carotenoid vesicles and pterinosomes were observed in both orange and brown morphs (Figure S5c,i).

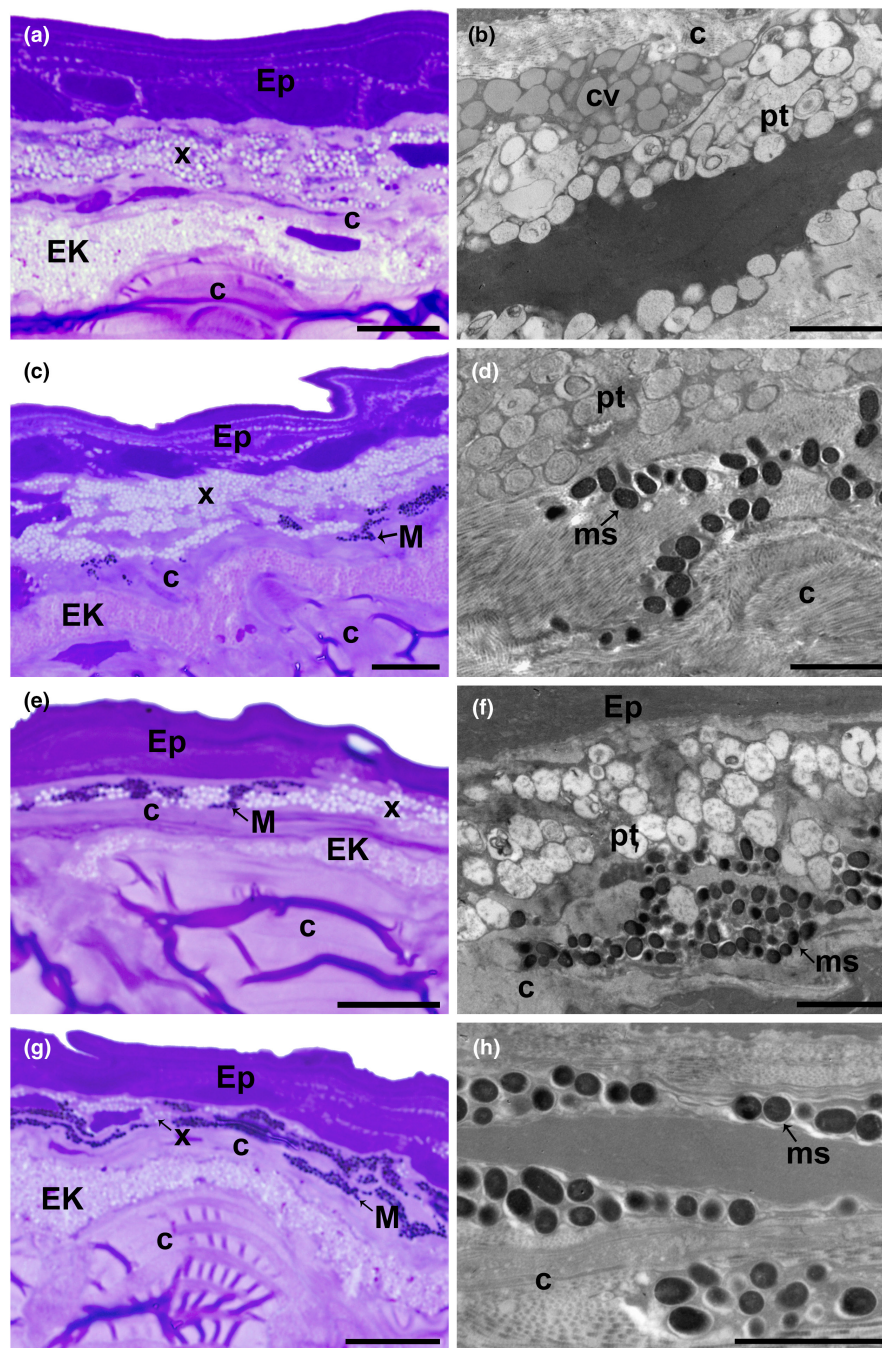


**FIGURE 2** Dorsal skin structure of *Brachycephalus actaeus* in transversal section highlighting chromatophores organization and distribution. Light microscope photomicrographs stained with toluidine blue (left) obtained with Olympus BX51 light microscope coupled to a DP71 digital camera and electron microphotographs (right) obtained with JEOL JEM 100CXII transmission electron microscope at 80 kV acceleration voltage. (a, b) Orange morphotype (JPCM1025); (c, d) grey morphotype (JPCM1062); (e, f) brown morphotype (JPCM1046) and (g, h) green morphotype (JPCM1033). C, collagen fibres; cv, carotenoid vesicle; EK, Eberth–Kastschenko; Ep, epidermis; M, melanophore; ms, melanosome; pt, pterinosome; x, xanthophore. Scale bar: a, c, e, g = 10 µm; b, d, f, h = 2 µm.

TABLE 1 Summary of skin layer measurements (in  $\mu\text{m}$ ) and chromatophores coverage (%)<sup>a</sup> of *Brachycephalus actaeus* morphs from dorsal and regions.

Trait	Dorsal				Ventral			
	Orange	Grey	Brown	Green	Orange	Grey	Brown	Green
Epidermis ( $\mu\text{m}$ )	9.68 $\pm$ 1.27 (3.54–14.00)	7.55 $\pm$ 1.49 (2.66–14.09)	10.29 $\pm$ 2.45 (5.88–16.43)	11.44 $\pm$ 3.99 (3.89–24.89)	7.43 $\pm$ 1.83 (3.96–12.46)	8.38 $\pm$ 0.71 (5.66–10.04)	9.21 $\pm$ 2.16 (3.35–16.72)	10.31 $\pm$ 2.38 (5.62–25.21)
Stratum spongiosum ( $\mu\text{m}$ )	13.56 $\pm$ 7.5 (5.41–35.98)	15.12 $\pm$ 8.45 (3.66–47.71)	25.63 $\pm$ 23.38 (5.67–81.03)	17.42 $\pm$ 9.51 (3.20–47.88)	11.85 $\pm$ 6.3 (3.20–32.05)	10.02 $\pm$ 9.88 (2.70–45.78)	10.19 $\pm$ 9.53 (2.24–68.18)	18.81 $\pm$ 12.17 (4.59–60.00)
EK ( $\mu\text{m}$ )	6.26 $\pm$ 2.91 (1.77–13.58)	3.74 $\pm$ 2.4 (0.65–13.77)	6.24 $\pm$ 3.76 (2.76–13.01)	7.76 $\pm$ 3.79 (1.63–19.61)	12.9 $\pm$ 6.89 (0.79–27.12)	16.69 $\pm$ 7.21 (4.94–33.68)	11.97 $\pm$ 9.64 (2.86–39.43)	13.09 $\pm$ 6.89 (3.26–42.23)
Stratum compactum ( $\mu\text{m}$ )	38.28 $\pm$ 4.11 (24.41–51.64)	26.93 $\pm$ 3.86 (16.07–47.58)	31.62 $\pm$ 7.83 (20.89–43.08)	48.03 $\pm$ 6.97 (18.39–80.38)	42.35 $\pm$ 9.45 (23.73–56.57)	28.74 $\pm$ 4.58 (22.99–44.23)	34.84 $\pm$ 6.47 (24.57–47.88)	42.26 $\pm$ 7.31 (18.54–77.90)
Melanophores coverage (%)	0.26 $\pm$ 0.26 (0–1.06)	1.52 $\pm$ 0.14 (1.38–1.66)	1.74 $\pm$ 1.47 (0.27–3.21)	7.97 $\pm$ 3.61 (3.59–12.43)	0	0	0	5.06 $\pm$ 2.61 (2.62–8.68)
Xanthophores coverage (%)	10.45 $\pm$ 8.06 (9.58–18.51)	8.78 $\pm$ 5.63 (3.16–14.41)	3.75 $\pm$ 2.99 (0.77–6.74)	2.23 $\pm$ 1.61 (0.20–4.14)	15.11 $\pm$ 3.41 (11.70–18.53)	7.43 $\pm$ 1.01 (6.42–8.44)	12.37 $\pm$ 8.61 (3.75–20.98)	2.61 $\pm$ 3.26 (0.13–7.22)

Note: Values are presented following mean  $\pm$  standard deviation (minimum–maximum).

<sup>a</sup>The area covered by melanosomes or xanthophores was divided by the total area of the chromatophore layer in each colour morph (see Materials and Methods).

### 3.3 | Reference transcriptome assembly and annotation

Assemblies with rnaSPADES and SOAPdenovo-trans produced the most complete transcript collections (Table S5, Figure S6). The entire collection of 8.9 million redundant transcripts was then reduced with EvidentialGene. The final consensus reference transcriptome (EvidentialGene's OK-group of transcripts) contained 764,760 transcripts with a N50 of 2098bp and a BUSCO score with 94.4% completeness, 1.5% fragmentation and 4.1% of missing genes (Table S5). Annotations with EnTap revealed that 405,769 transcripts had open reading frames (ORFs) and 251,354 had a hit against UniProt or RefSeq protein sequence databases. Only 6651 out of 764,760 transcripts were flagged as contaminants in this annotation pipeline and excluded for subsequent analyses. Gene family and ontology searches against the EggNOG database assigned 252,134 transcripts to gene families. Together with similarity searches against *X. tropicalis* proteome and Uniprot protein databases, it allowed the functional annotation of 263,618 transcripts.

### 3.4 | Genetic structure

We recovered a total of 78,819 SNPs in the superTranscriptome of *B. actaeus*. Of these, 23,579 bi-allelic SNPs were used for population structure analysis (Figure 3). The PCA based on SNPs showed three clusters composed of two mainland groups: (1) BNb and BNg; (2) CAS, CAG and GLO and (3) the island population SPA (Figure 3c). The SPA samples were distinct from others in the first and second components, explaining 21.13% of the variance. The Admixture analysis exhibited the best-fit *K* value for two populations: one containing island samples (SPA) and another with all other samples (BNb, BNg, CAS, CAG and GLO; Figure 3c and Figure S7). The *K* value for three recovered the same population structure as PCA (Figure 3b,c). In both analyses, the populations were not structured by colour morphs.

### 3.5 | Differential expression analyses

Expression values from 79,567 transcripts from 12,943 genes with functional annotation and expressed above the cut-off values were used for differential expression testing among the colour phenotypes. The PCA plot of log2-transformed TPM normalized gene expression estimates showed a noteworthy level of clustering of samples by locality, with samples from SPA followed CAS showing the most significant divergence from the rest (Figure S8). Also, the PCA of gene expression did not present a colour morph structure. 3DRNASeq pairwise and one-versus-all contrasts between colour phenotypes identified 454 DEGs. Among these, we identified 26 colour-associated DEGs. Eight of these were genes from the melanin synthesis pathway (*pmel*, *edn1*, *wnt9a*, *dct*, *slc24a5*, *tyrp1*, *oca2*, *egfr*),



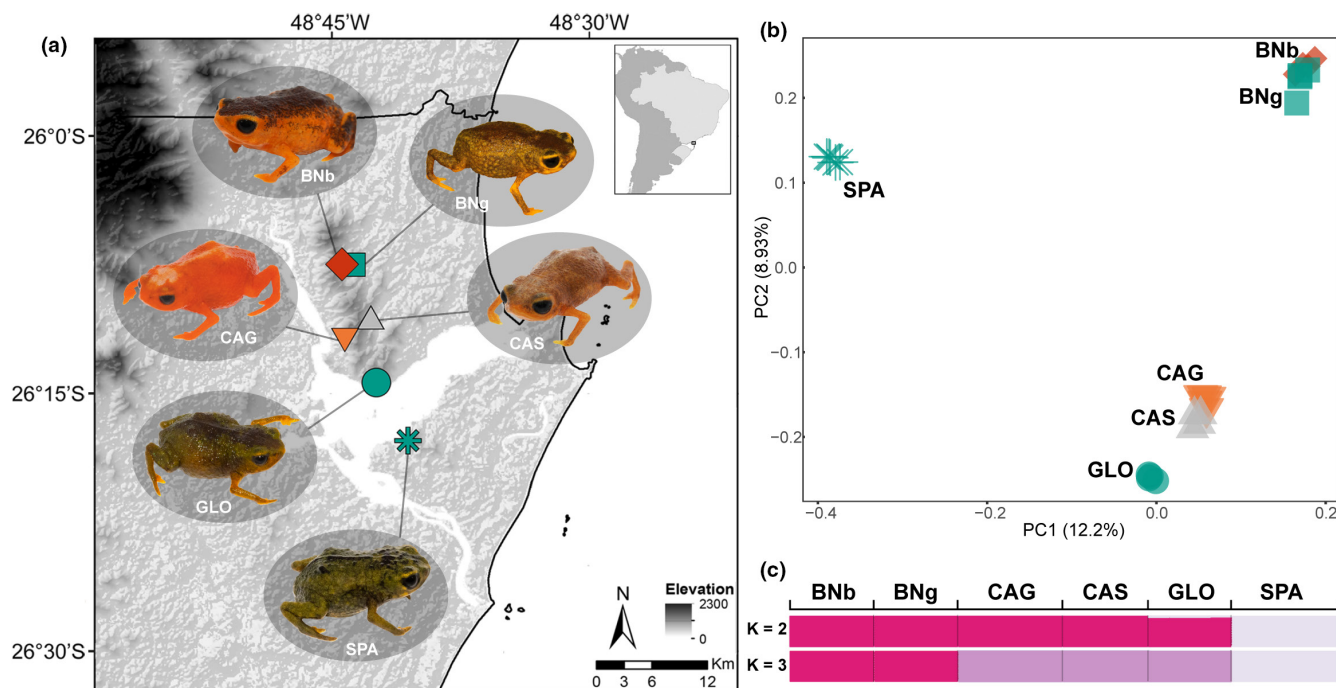


**FIGURE 3** General genetic structure through geographic distribution of *Brachycephalus actaeus* colour morphs northeastern state of Santa Catarina, Brazil. (a) Topographic map indicating the geographic location of the colour morphs and their corresponding symbols: Diamond=BNb, Alto Braço do Norte, brown morph; square=BNg, Baixo Braço do Norte, green morph; inverted triangle=CAG, Cantagalo, orange morph; triangle=CAS, Casarão, grey morph; circle=GLO, Vila da Glória, green morph; and asterisk=SPA, Serra da Palha, green morph. (b) Scores of 23,579 bi-allelic SNPs from 26 individuals in the first two principal components. (c) Population structure estimated with Admixture software for models with 2–3 ancestral populations (K). Ancestry proportions are represented by pink gradient bars (best-fit model K=2). The colours of symbols represent the colour morph classification.

two from the melanosome transport and biogenesis (*mlana*, *mreg*), two DEGs are linked to the carotenoid metabolism (*aldh1a2*, *rpe65*) and one DEG of the purine synthesis pathway (*gart*). In addition, we found 13 other DEGs previously linked to chromatophore differentiation in vertebrates (Figure 4; Table 2).

The DEGs in the melanin synthesis pathway showed four different expression profiles: three genes (*oca2*, *slc24a5*, *tyrp1*) were down-regulated in orange toadlets and up-regulated in green and, to a lesser extent, brown and grey toadlets; the other four (*dct*, *edn1*, *mlana*, *pmel*) were down-regulated in orange and brown toadlets and up-regulated in grey and green toadlets; only one gene (*wnt9a*) was exclusively down-regulated in orange toadlets and only one gene (*mreg*) was exclusively up-regulated in orange and, to a lesser extent, in green toadlets (Table 2).

The two DEGs associated with the carotenoid metabolism showed up-regulation in grey toadlets. For *rpe65*, this up-regulation was pronounced and all the three other colour morphs were down-regulated, but for *aldh1a2*, some up-regulation was detected in green toadlets as well. The purine synthesis enzyme *gart* gene, associated with iridophore-based pigmentation, was up-regulated in brown and grey colour phenotypes and down-regulated in orange and green ones.

Among all the DEGs between colour morphs of *B. actaeus* identified in this study, 115 out of 454 (25% of the DEGs) also appeared in one or more published lists of DEGs among colour morphs of *D.*

*auratus*, *O. pumilio* and *R. sirensis*. Interestingly, only 12 genes in this group, supported by cumulative evidence, have been previously linked to pigmentation in vertebrates, while the other 103 genes have no known association with pigmentation (Table S6).

### 3.6 | Linking gene expression to predator perceptual space

Expression filtering across the expression matrix of 25,142 genes, based on functional annotation (263,618 transcripts), in 26 individuals of *B. actaeus* removed 9858 low-expressed genes and the remaining 15,284 genes were included in *Olivia* expression association analyses. For the x-axis values, 18 candidate genes were identified, of which five are pigmentation associated. Four genes participate in the melanin synthesis pathway (*dct*, *oca2*, *slc24a5*, *tyrp1*) and one in the melanosome biogenesis (*mlana*). All these melanosome-associated genes decrease their expression as the x-axis scores increase (Table 3, Figure S9). Analyses with luminance values as predictors did not identify any expression-associated genes. Only 10 genes, including the five above-mentioned melanin-related genes, were shared between the regression-based expression association analysis (*Olivia*) and the classical differential gene expression tests implemented in 3DRNASeq (section 3.5). The proportion of coloration related genes among

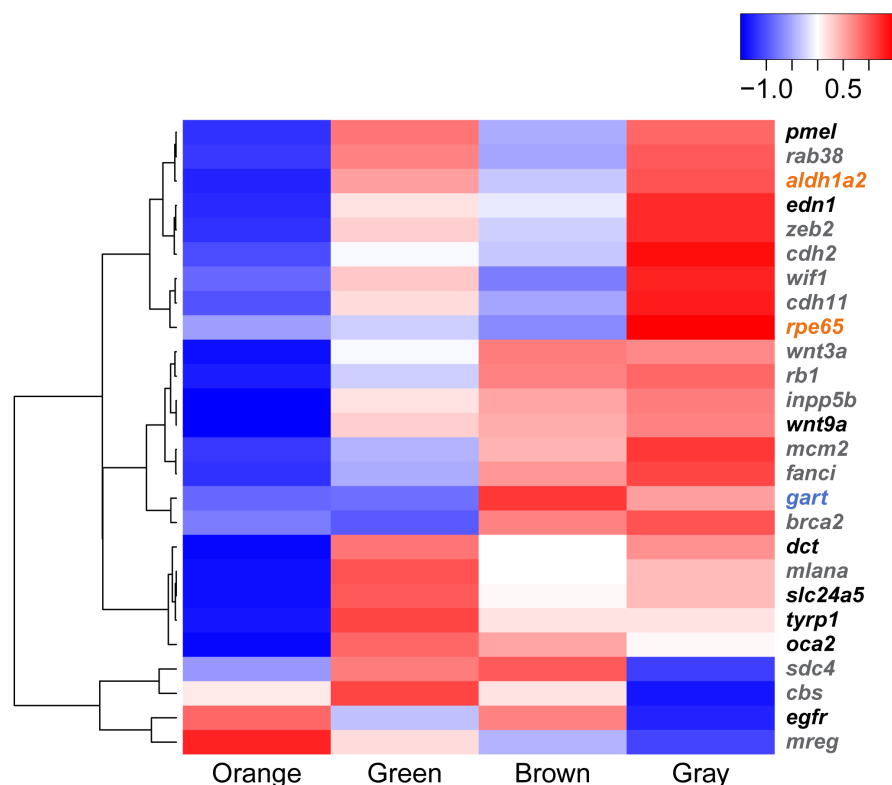


**FIGURE 4** Expression patterns of colour-associated genes in four colour morphs categories of *Brachycephalus actaeus*. The heatmap plot represents the averaged expression values of all genes across all samples in each morph. Twenty-six differentially expressed genes are highlighted following functional groups: Melanin synthesis (in black), carotenoid metabolism (in orange), iridophores in guanine synthesis (in blue) and other pigmentation associated genes (in grey).

the statistically significant genes detected by each method was, however, much higher in the *Olivia* results (5/18, 28%) than in the 3DRNASeq results (26/454, 5.7%).

### 3.7 | Gene co-expression network analyses

The WGCNA identified 32 gene modules, five significantly correlated with the coloration variables (four with colour and one with luminance). Albeit statistically significant, all these correlations were relatively weak ( $-0.43 < r < .51$ ) (Figure S10), and we interpreted them with caution. Magenta and royal blue modules showed the strongest correlations with the colour variable, while the tan module showed the strongest correlation with the luminance variable. Among the 967 genes in the magenta module, the five most overrepresented biological functions were very generic: nitrogen compound metabolic process (GO:0006807), metabolic process (GO:0008152), primary metabolic process (GO:0044238), organic substance metabolic process (GO:0071704) and cellular nitrogen compound metabolic process (GO:0034641). In the royal blue module, only the transposition (GO:0032196) was overrepresented, while in the tan module, no statistically significant overrepresentation was detected. The other two modules statistically correlated with coloration variables, light cyan and midnight blue, were also overrepresented with generic biological processes like primary metabolic process (GO:0044238), metabolic process (GO:0008152), nitrogen compound metabolic process (GO:0006807), cellular metabolic process (GO:0044237) and organic substance metabolic process (GO:0071704).

As expected, the average DEGs content of the five colour-correlated modules (2.5% of DEGs in the modules) nearly doubled that of the uncorrelated modules (1.3%). The representation of colour-related genes (from our a priori list, see Methods) in the modules was, however, not different between the five colour-correlated modules (3.6%) and uncorrelated modules (3.4%).

## 4 | DISCUSSION

In amphibians, the genetic mechanism underlying colour variation has barely been studied, particularly in non-model species (Rodríguez et al., 2020; Stuckert et al., 2023; Twomey, Johnson, et al., 2020). Our study on *Brachycephalus actaeus* provides the first insight into the molecular basis of colour polymorphism in a small Neotropical toadlet of the family Brachycephalidae, likely representing the lowest size limit of colour polytypism in tetrapods.

### 4.1 | Ecological and evolutionary implications of polytypism in *B. actaeus*

Intra-specific colour variation (polymorphism and polytypism) in anurans has been associated with diurnal activity, conspicuous colorations and toxicity (Wollenberg et al., 2008). In particular, polytypism in poison frogs has been suggested as a strategy for balancing detection costs by different predators (Pröhl & Ostrowski, 2011; Willink et al., 2013). This scenario is usually interpreted within the aposematic and cryptic antipredator strategies, in which a species utilizes

TABLE 2 Differentially expressed genes across *Brachycephalus actaeus* skin colour morphs with previous links to colour variation.

Gene symbol	Gene name	Pathway	Contrast group	Regulation state	q	log2FC
dct	L-Dopachrome tautomerase precursor	Melanin synthesis	Orange–grey	Down-regulated	0.021	–3.769
edn1	Endothelin-1	Melanin synthesis	Orange–grey	Down-regulated	0.010	–1.758
pmel	Melanocyte protein PMEL isoform X1	Melanin synthesis	Orange–grey	Down-regulated	0.009	–2.674
dct	L-Dopachrome tautomerase precursor	Melanin synthesis	Orange–green	Down-regulated	0.006	–4.290
oca2	P Protein isoform X1	Melanin synthesis	Orange–green	Down-regulated	0.049	–7.942
pmel	Melanocyte protein PMEL isoform X1	Melanin synthesis	Orange–green	Down-regulated	0.003	–2.736
dct	L-Dopachrome tautomerase precursor	Melanin synthesis	Orange– (green + brown + grey)	Down-regulated	0.017	–3.584
edn1	Endothelin-1	Melanin synthesis	Orange– (green + brown + grey)	Down-regulated	0.038	–1.187
pmel	Melanocyte protein PMEL isoform X1	Melanin synthesis	Orange– (green + brown + grey)	Down-regulated	0.015	–2.096
wnt9a	Protein Wnt-9a isoform X1	Melanin synthesis	Orange– (green + brown + grey)	Down-regulated	0.040	–1.239
edn1	Endothelin-1	Melanin synthesis	Grey– (orange + green + brown)	Up-regulated	0.029	1.158
pmel	Melanocyte protein PMEL isoform X1	Melanin synthesis	Green–brown	Up-regulated	0.048	1.858
dct	L-Dopachrome tautomerase precursor	Melanin synthesis	Green– (orange + brown + grey)	Up-regulated	0.009	2.136
pmel	Melanocyte protein PMEL isoform X1	Melanin synthesis	Green– (orange + brown + grey)	Up-regulated	0.018	1.552
slc24a5	Sodium/potassium/calcium exchanger 5 isoform X1	Melanin synthesis	Green– (orange + brown + grey)	Up-regulated	0.024	2.748
tyrp1	5,6-Dihydroxyindole-2-carboxylic acid oxidase precursor	Melanin synthesis	Green– (orange + brown + grey)	Up-regulated	0.041	3.807
oca2	P Protein isoform X1	Melanin synthesis	Green– (orange + brown + grey)	Up-regulated	0.013	4.325
wnt3a	Protein Wnt-3a	Pigmentation variation	Orange–brown	Down-regulated	0.038	–1.306
cdh2	Cadherin-2 precursor	Pigmentation variation	Orange–grey	Down-regulated	0.033	–2.495
cdh11	Cadherin-11 precursor	Pigmentation variation	Orange–grey	Down-regulated	0.018	–1.939
egfr	Epidermal growth factor receptor	Pigmentation variation	Orange–grey	Up-regulated	0.021	1.061
fanci	Fanconi anaemia group I protein	Pigmentation variation	Orange–grey	Down-regulated	0.031	–1.622
mcm2	DNA replication licensing factor mcm2	Pigmentation variation	Orange–grey	Down-regulated	0.024	–2.193
mlana	Melanoma antigen recognized by T-cells 1 isoform X1	Pigmentation variation	Orange–grey	Down-regulated	0.045	–1.716
rb1	Retinoblastoma-associated protein	Pigmentation variation	Orange–grey	Down-regulated	0.028	–1.985
wif1	Wnt inhibitory factor 1 precursor	Pigmentation variation	Orange–grey	Down-regulated	0.024	–1.534
wnt3a	Protein Wnt-3a	Pigmentation variation	Orange–grey	Down-regulated	0.028	–1.221

(Continues)

TABLE 2 (Continued)

Gene symbol	Gene name	Pathway	Contrast group	Regulation state	q	log2FC
zeb2	Zinc finger E-box-binding homeobox 2 isoform X1	Pigmentation variation	Orange-grey	Down-regulated	0.003	-2.054
mlana	Melanoma antigen recognized by T-cells 1 isoform X1	Pigmentation variation	Orange-green	Down-regulated	0.001	-2.570
mreg	Melanoregulin isoform X1	Pigmentation variation	Orange-green	Up-regulated	0.044	1.471
rab38	Ras-related protein Rab-38	Pigmentation variation	Orange-green	Down-regulated	0.038	-1.990
zeb2	Zinc finger E-box-binding homeobox 2 isoform X1	Pigmentation variation	Orange-green	Down-regulated	0.024	-1.352
inpp5b	Type II inositol 1,4,5-trisphosphate 5-phosphatase isoform X1	Pigmentation variation	Orange-(green + brown + grey)	Down-regulated	0.046	-1.268
mlana	Melanoma antigen recognized by T-cells 1 isoform X1	Pigmentation variation	Orange-(green + brown + grey)	Down-regulated	0.013	-1.859
mreg	Melanoregulin isoform X1	Pigmentation variation	Orange-(green + brown + grey)	Up-regulated	0.012	2.065
rb1	Retinoblastoma-associated protein	Pigmentation variation	Orange-(green + brown + grey)	Down-regulated	0.038	-1.598
wnt3a	Protein Wnt-3a	Pigmentation variation	Orange-(green + brown + grey)	Down-regulated	0.012	-1.152
zeb2	Zinc finger E-box-binding homeobox 2 isoform X1	Pigmentation variation	Orange-(green + brown + grey)	Down-regulated	0.016	-1.371
brca2	Breast cancer type 2 susceptibility protein isoform X4	Pigmentation variation	Green-grey	Down-regulated	0.045	-1.225
cbs	Cystathionine beta-synthase isoform X2	Pigmentation variation	Green-grey	Up-regulated	0.016	1.284
sdca4	Syndecan 4 precursor	Pigmentation variation	Green-grey	Up-regulated	0.050	1.271
mlana	Melanoma antigen recognized by T-cells 1 isoform X1	Pigmentation variation	Green-(orange + brown + grey)	Up-regulated	0.004	1.568
cdh2	Cadherin-2 precursor	Pigmentation variation	Grey-(orange + green + brown)	Up-regulated	0.024	1.857
cdh11	Cadherin-11 precursor	Pigmentation variation	Grey-(orange + green + brown)	Up-regulated	0.026	1.461
wif1	Wnt inhibitory factor 1 precursor	Pigmentation variation	Grey-(orange + green + brown)	Up-regulated	0.031	1.232
zeb2	Zinc finger E-box-binding homeobox 2 isoform X1	Pigmentation variation	Grey-(orange + green + brown)	Up-regulated	0.009	1.367
aldh1a2	Retinal dehydrogenase 2	Carotenoid metabolism	Orange-grey	Down-regulated	0.034	-1.672
rpe65	Retinoid isomerohydrolase	Carotenoid metabolism	Grey-(orange + green + brown)	Up-regulated	0.030	1.438
gart	Trifunctional purine biosynthetic protein adenosine-3	Guanine synthesis in iridophores	Green-brown	Down-regulated	0.042	-1.124

Note: The regulation state is always referred to the first term of the comparison.

conspicuous coloration to advertise toxic compounds or colours that mimic the environment to reduce the possibility of being detected by a potential predator respectively (Caro & Ruxton, 2019; Rojas et al., 2015; Ruxton et al., 2018). Given the presence of tetrodotoxin

in some species of pumpkin toadlets (Chimetto Tonon et al., 2021; Pires et al., 2005) and the diurnality of the genus, the bright orange morphs of *B. actaeus* can be reasonably interpreted in terms of aposematic signal. However, there is no data on the presence of



tetrodotoxin in *B. actaeus*, precluding a selective predation pressure based on colour variation and a crypsis/aposematic strategy.

In addition, although birds are considered one of the main predators of frogs (e.g. Casas-Cardona et al., 2018; Dreher et al., 2015; Maan & Cummings, 2012), there is only one report of predation in *Brachycephalus* by a tinamou (Carvalho, 1940). This lack of information also prevents an understanding of how the colour variation from *B. actaeus* is perceived by other potential predators and, with it, whether the predator community is indeed exerting selective pressure on this trait. Natural history observations and predation experiments need to be conducted to clarify the role of predation in shaping colour variation in *B. actaeus*. This should include consideration of other visually oriented predators such as crabs, spiders, mammals, lizards and other anurans.

An alternative scenario to explain colour variation in *B. actaeus* is intra-specific social interactions. The presence of distinct opsins in the retina of *Brachycephalus* and other diurnal frogs enables the perception of wavelength sensitivity, resulting in colour discrimination (Wan et al., 2023; Yovanovich et al., 2017). For instance, dorsal coloration was revealed to be important for male competition and female mating preference in *O. pumilio* (Maan & Cummings, 2008), and it was shown that colour variation could also be related to sexual selection (Crothers et al., 2011; Palacios-Rodríguez et al., 2022). However, the inter- and intra-specific colour communication and signalling in *Brachycephalus* remains unstudied (see Pombal et al., 1994). A third alternative scenario to explain this polytypism can be random genetic drift, given the likely isolation of some populations of *B. actaeus* (Chouteau & Angers, 2012; Mallet & Joron, 1999; Reynolds & Fitzpatrick, 2007).

## 4.2 | Population structure

Our results indicate that colour variation in *B. actaeus* populations is not linked to genetic structure but to geographic barriers and distances between populations. Similar patterns of genetic structure have been found for other polytypic frogs (Rojas et al., 2020; Roland et al., 2017). The population from São Francisco do Sul Island (SPA) is the most genetically distinct, likely due to geographic isolation by the Babitonga Bay. Despite this isolation, genetic distances between clusters remain relatively low on mitochondrial markers (Monteiro et al., 2018), suggesting recent isolation. The mainland cluster is further divided into two genetic groups that follow the geographic proximities (see Figure 3), each containing different coloured populations. The genetic differences observed in these two groups may be influenced by distance, low vagility and species-specific microhabitat preferences (Pie et al., 2013), though further studies are needed to address this question. In addition, the sampling gap among these localities may overshadow a clinal pattern of genetic variation.

As discussed in the previous section, the lack of information on toxin profile and natural history hampers solid bases for understanding the origin and maintenance of distinct coloured populations in *B.*

*actaeus*. Previous works on polytypic frogs suggested that natural and/or sexual selection is not required to increase and maintain colour variation (Lehman et al., 2024; Yeager et al., 2023). In fact, in species with small population sizes, which might be the case of the studied species, phenotype fixation may occur randomly through genetic drift (Chouteau & Angers, 2012). Further research on ecology and population genetics is needed to shed light on the roles of selection and drift in maintaining colour polytypism in *B. actaeus*. These findings also underscore the importance of re-evaluating the inclusion of only coloration as a diagnostic character in new species descriptions of *Brachycephalus* (Pie et al., 2018; Ribeiro et al., 2017), particularly in cases with low genetic distances or lack of genetic data. Therefore, we emphasize the necessity of incorporating population genetic variation into the taxonomic context.

## 4.3 | Insights into skin structural and ultrastructural analyses

Histological examinations allowed us to trace the observed skin colour variation of *B. actaeus* to the distribution of chromatophores. Specifically, the scarce number or complete absence of melanophores in the orange morphs, along with their more aggregated distribution in the brown, followed by the grey and green morphs, supports a pivotal role of melanin in the colour variation observed in this species. We also documented differences in the location of melanophores above and among xanthophores in the green and brown morphs and basal to the xanthophores in the grey morph. Xanthophores were more abundant in the orange skin and contained carotenoids and pteridines (pterinosomes) (Figure 3). These findings align with recent studies on the European fire salamander (*Salamanca salamandra bernardezi*), where melanophores are more abundant in black than brown skin and are rare in yellow skin (Burgon et al., 2020).

In a model proposed by Bagnara and Matsumoto (2006), they used a differential light absorbance and reflecting phenomena generated by the three chromatophore layers to explain the amphibian skin colour perceived by a human observer. In this model, green coloration is derived from the interaction of these three layers. In contrast, although not explicitly mentioned, an orange/reddish coloration might be derived from the reflection of these wavelengths in other tissue or cell components and the absence of melanophores. Notably, we did not identify iridophores in the skin of any *B. actaeus* morphs. Thus, our results support this model for the orange coloration perceived in *B. actaeus*, though the component responsible for orange/reddish reflection is still unresolved, while it suggests that the green colour is derived from a different phenomenon. Since green coloration is one of the most studied colours in amphibians, our findings, along with recent publications on the role of biliverdin and biliverdin-binding proteins in tree frogs (Taboada et al., 2020), reveal that we still ignore many aspects of amphibians' coloration.

Gene	AdjLogFC	SE	T-stat.	df	p	BH FDR	Emp. p	BH p
<b>tyrp1</b>	-1.254	0.128	-9.796	23	.000	0.000	.000	.001
<b>slc24a5</b>	-0.968	0.141	-6.865	23	.000	0.003	.000	.001
<b>dct</b>	-0.885	0.154	-5.747	23	.000	0.019	.000	.013
<b>c7h10orf95</b>	-0.724	0.146	-4.972	23	.000	0.045	.000	.045
<b>oca2</b>	-0.714	0.092	-7.747	23	.000	0.001	.000	.001
<b>yipf7</b>	-0.495	0.096	-5.153	23	.000	0.037	.000	.035
<b>bmp2</b>	-0.492	0.100	-4.902	23	.000	0.051	.000	.049
<b>mlana</b>	-0.471	0.086	-5.483	23	.000	0.023	.000	.019
<b>ppp1r3c.2</b>	-0.449	0.088	-5.134	23	.000	0.037	.000	.035
<b>sik1</b>	-0.416	0.082	-5.102	23	.000	0.037	.000	.038
<b>klhdc7b</b>	-0.390	0.060	-6.528	23	.000	0.004	.000	.001
<b>jun_2</b>	-0.250	0.045	-5.579	23	.000	0.023	.000	.019
<b>lca5</b>	-0.183	0.037	-4.975	23	.000	0.045	.000	.045
<b>znf574</b>	0.119	0.023	5.150	23	.000	0.037	.000	.035
<b>derl3</b>	0.205	0.037	5.464	23	.000	0.023	.000	.019
<b>jmjd7</b>	0.279	0.053	5.260	23	.000	0.034	.000	.029
<b>LOC116412396</b>	1.286	0.220	5.854	23	.000	0.018	.000	.013
<b>cdhr3_3</b>	1.286	0.234	5.490	23	.000	0.023	.000	.019

Note: Genes related to pigmentation variation are highlighted in bold.

Abbreviations: AdjLogFC, adjusted log-fold change per unit increase of x-coordinate scores (increase = more orange-red coloration); BH FDR, Benjamini-Hochberg false detection ratio; BH p, Benjamini-Hochberg corrected p-value; df, degrees of freedom; Emp. p, empirical p value; SE, standard error; T-stat., T-statistic of regression model.

**TABLE 3** Results of the transcriptome-wide association analysis with *Olivia* software relating gene expression change and the scores of individual *Brachycephalus actaeus* in the x-coordinate of bird perceptual space.

#### 4.4 | Gene expression differences between colour morphs

In general, previous studies in vertebrates have associated darker colours (brown or green) with a greater expression of melanin genes (Henning et al., 2013; McNamara et al., 2021). By contrast, orange colour has been frequently correlated with carotenoid and pteridine genes (Andrade & Carneiro, 2021; Hubbard et al., 2010). Surprisingly, most genes identified in our study were directly or indirectly related to the melanin pathway (19 out of 26). These included significant members of the tyrosinase family (*dct*, *pmel*, *tyrp1*) and melanosome biogenesis or transporter genes (*oca2*, *slc24a5*, *mlana*, *mreg*) (Braasch et al., 2007). We conclude that colour variation in *B. actaeus* mainly derives from the differential regulation of melanin production. These results were also concordant with the morphological configuration of the skin revealed in our histological analyses. Finally, given the limited number of colour-related genes in our results, we briefly examine each gene's contribution, indexed by sub-sections next.

The overlap between our list of DEGs and those in other hyloidean species points to candidate genes for colour variation specific to anurans. Of particular interest is a subset of 12 genes (*adamtsl4*, *aldh9a1*, *ccdc80*, *col6a3*, *egfr*, *fat4*, *mrc2*, *pdgfra*, *pnp*, *pnrc2*, *slc29a1* and *tyrp1*) which have been found differentially expressed between colour morphs in three separate studies including ours. Except for *egfr* and *tyrp1*, genes in this list have not previously been associated with pigmentation in other vertebrates and should be the focus of

future studies on amphibians. The collagen alpha-3(VI) chain gene (*col6a3*) is an exciting candidate as the role of the dermic collagen arrays in the pigmentation of anurans has been experimentally verified (Bagnara et al., 2007), but the underlying genetic mechanism is yet to be uncovered.

##### 4.4.1 | Melanin synthesis and pigment-associated genes

In vertebrates, melanin is well established to be the primary pigment of darker skin, fur and feathers (Braasch et al., 2007; Hofreiter & Schöneberg, 2010; Mills & Patterson, 2009). Accordingly, we found a suite of differentially expressed melanin-related genes that contribute to skin pigmentation in the brown, grey, green and orange colour morphs of *B. actaeus*.

Overall, DEGs that were identified to be involved in melanin synthesis were down-regulated or undetectable in orange skin (see next), and this observation matches the lack of or little melanophores in skin structural and ultrastructural analyses. The only higher expressed gene in orange versus all morphs was *mreg*, which plays a role in melanosome transport and is involved in pigmentation (Stuckert et al., 2019). *mreg* was found differentially expressed across colour morphs of *D. auratus*, but without any noticeable colour association (Stuckert et al., 2019). In fishes, *mreg* was positively related to dark colours (Henning et al., 2013). Also, the orange and

brown morphs showed the gene *egfr* up-regulated, while in the grey and green morphs, it is down-regulated. Its contribution to orange pigmentation is unknown.

We found a profile of up-regulation of DEGs relating to melanin synthesis contributing to grey and green coloration. Interestingly, the DEGs profile found in the green morph is related to melanosome formation (*dct*, *oca2*, *mlana*, *pmel*, *slc24a5* and *tyrp1*), whereas in the grey morph, DEGs profile likely plays a role in melanin regulation/concentration (*cdh11*, *cdh2*, *edn1*, *wif1* and *zeb2*). This pattern is supported by the skin structural and ultrastructural analyses.

The expression patterns of the melanosome formation genes *dct*, *tyrp1* and *pmel* found in the green morph agree with that observed in non-amphibian vertebrates with dark coloration (Higdon et al., 2013; Hoekstra, 2006; McNamara et al., 2021). *dct* (also known as *tyrp2*) and *tyrp1* stimulate the production of eumelanin (McNamara et al., 2021; Vachtenheim & Borovanský, 2010). *pmel* (also known as *silv* or *pmel17*) is involved in melanosome formation, promoting a fibrillar matrix in the melanosome cell to optimize the sequestration and condensation of melanin pigment (McNamara et al., 2021). Further, the green morph shows the genes *oca2* and *slc24a5* up-regulated, which encode proteins that maintain the ionic stability of the processes during melanosome maturation (Braasch et al., 2007; Lamason et al., 2002).

Furthermore, we identified in the green morph the genes *mlana* (also known as *mart-1* and *melan*) and *rab38* were higher expressed. *mlana* is a crucial element controlling the expression of *pmel*, which displays a critical role in melanosome formation (Hoashi et al., 2005). This matches perfectly with the expression profile observed in our study and supports the role of *mlana* for melanin control in the green skin of *B. actaeus*. Correspondingly, *mlana* and *pmel* were down-regulated in yellow skin compared to black skin in European fire salamander (Burgon et al., 2020). *rab38* encodes a protein rab38, playing a significant role in sorting the melanosomal protein *tyrp1*. Mutational forms cause brown pigmentation in mice (Loftus et al., 2002).

The green versus grey morph shows an unexpected up-regulated gene. The *cbs* gene is linked to pheomelanin synthesis, a key factor for red skin formation (Fang et al., 2022; Zhu et al., 2016). Pheomelanin is an alternative product of the melanin synthesis pathway (e.g. Megía-Palma et al., 2018; Wolnicka-Glubisz et al., 2012). In lizards, pheomelanin was detected in brownish, grey and black skin coloration (Megía-Palma et al., 2018). Supplementary studies are needed to evaluate the presence of pheomelanin in *Brachycephalus* and the function of associated genes.

Remarkably, most pre-melanosome genes were highly expressed in the grey morph (*brca2*, *cdh2*, *cdh11*, *edn1*, *wif1*, *wnt3a*, *wnt9a* and *zeb2*). In the initial stages of cell development, *edn1* mediates a specific signalling pathway that modulates melanin synthesis, regulating the production or distribution of melanin in the skin (Braasch & Scharl, 2014). *zeb2*, *cdh2* and *cdh11* play a role in cell adhesion, regulation and migration, all influencing melanocyte differentiation (Higdon et al., 2013; Maître & Heisenberg, 2013). Many of these DEGs, *brca2*, *wif1*, *wnt9a*, *egfr* and *wnt3a*, are from

several key signalling pathways preceding melanogenesis (Bagnara & Matsumoto, 2006). Precisely, they directly affect the transcriptional activity of the MIFT block, called the master regulator of melanocyte development, which has a pivotal control in melanogenesis and regulates the expression of the main melanogenic enzymes (Bagnara & Matsumoto, 2006; McLean et al., 2017; McNamara et al., 2021). In *O. pumilio*, the *wnt9a* gene was up-regulated in red and green morphs in contrast to blue (Rodríguez et al., 2020). Finally, we also found the gene *rb1* up-regulated in the grey morph; *rb1* is fundamental for the cell cycle progression of melanocytes and is a tumour suppressor gene (Carreira et al., 2005). Although this gene was recovered in research on other amphibians, its association with colour variation is still unclear (Stuckert et al., 2019).

The DEGs' profiles described here differ from studies in the poison frogs *D. auratus* and *Oophaga histrionica*, which have assigned *mc1r* a role in colour variation (Posso-Terranova & Andrés, 2017; Stuckert et al., 2019). In *O. pumilio*, *mc1r*, *kit* and *tyrp1* are higher expressed in dorsal (green) coloration, whereas *asip* and *tyr* are higher expressed in ventral (yellow) (Stuckert et al., 2023). Another study in *O. pumilio* shows *oca2* up-regulated in blue compared to green and red morphs (Rodríguez et al., 2020). Our results allow us to propose the functional involvement of these melanin-candidate genes in the colour morphs of *B. actaeus*. To provide a more precise understanding, we depicted the functions of these genes in melanin synthesis (Figure 5).

#### 4.4.2 | Genes involved in carotenoid metabolism and purine synthesis

The grey morph of *B. actaeus* shows two up-regulated genes (*aldh1a2*, *rpe65*) involved in carotenoid metabolism. Despite not being directly associated with chromatophores, both genes can influence the regulation of melanocyte stem cells, as well as melanocyte differentiation and proliferation (Amann et al., 2012; VanBuren & Everts, 2022). *aldh1a2* was found higher expressed in green (dorsal) than yellow (ventral) skin coloration during the early development of *O. pumilio* (Stuckert et al., 2023). Gene members from the *aldehyde dehydrogenase 1* family (*aldh1a1* and *aldh1a3*) are associated with blue/green colour in frogs (Rodríguez et al., 2020) and red/yellow or blue skin colour of lizard species (McLean et al., 2017, 2019; Nicolai et al., 2021). The gene *rpe65* primarily plays a crucial role in the visual cycle and is essential for rod and cone photoreceptors (VanBuren & Everts, 2022).

The single gene involved in purine synthesis, *gart*, was higher expressed in brown than in green morphs of *B. actaeus*. In *O. pumilio*, *gart* and other genes, which code for enzymes influencing guanine production, showed higher expression in blue frogs (Rodríguez et al., 2020), whereas in *D. auratus*, the *gart* gene was expressed at low levels in the 'green microspot' population (Stuckert et al., 2019). In zebrafish, *gart* mutants present pigmentation defects and microphthalmia, displaying invisible xanthophores and iridophores, while melanophore pigmentation is

## Melanocyte development

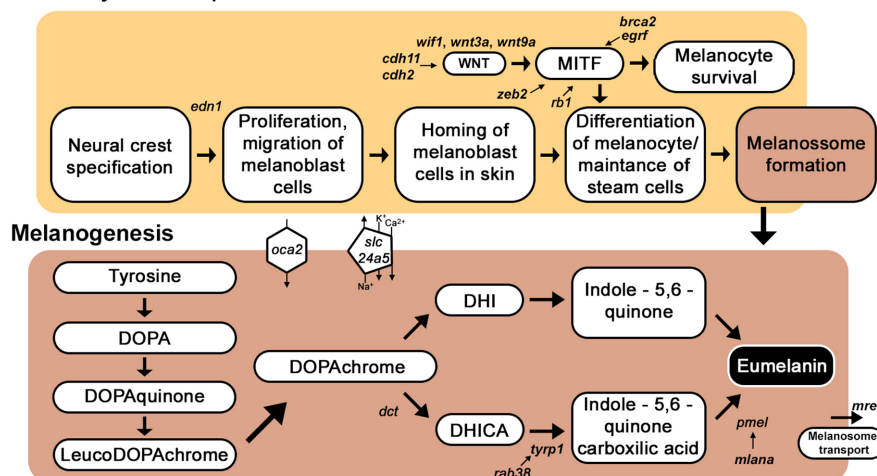


**FIGURE 5** Summary of regulatory effects detected on the melanin pathway in *Brachycephalus actaeus*. Steps of the melanocyte development and melanogenesis pathways (adapted from Braasch et al. (2007) and Cieslak et al. (2011)) were annotated with the differentially expressed genes identified in our study (in italics) and their putative roles. WNT and MITF are transcription regulators. Gene names: *Brca2*, BRCA2 DNA repair associated; *cdh11*, cadherin 11; *cdh2*, cadherin 2; *dct*, dopachrome tautomerase; *edn1*, endothelin 1; *egfr*, epidermal growth factor receptor; *mlana*, melan-A; *mreg*, melanoregulin; *oca2*, oculocutaneous albinism II; *pmel*, premelanosome protein; *rab38*, ras-related protein Rab-38; *rb1*, retinoblastoma-associated protein; *slc24a5*, solute carrier family 24 member 5; *tyrp1*, tyrosinase-related protein 1; *wif1*, WNT inhibitory factor 1; *wnt3a*, Wnt family member 3A; *wnt9a*, wingless-type MMTV integration site family member 9A; *zfb2*, zinc finger E-box binding homeobox 2.

reduced (Ng et al., 2009). The genes *aldh1a2*, *rpe65* and *gart* were lower expressed in the orange morph of *B. actaeus*, likely assisting the regulation and playing a functional link with the melanin synthesis genes. The contradiction between the gene expression in guanine synthesis and the lack of iridophores suggests that these genes may also be implicated in other pathways or that the purines accumulate in other chromatophores.

In contrast with melanin, the genetic mechanisms underlying carotenoids and, especially, pteridine pigments are poorly characterized (Andrade & Carneiro, 2021). These candidate genes are essential for producing yellow, orange or red pigmentation in several amphibians (Bagnara & Hadley, 1969; Rodríguez et al., 2020; Twomey, Johnson, et al., 2020; Twomey, Kain, et al., 2020). For example, a carotenoid ketolase gene more highly expressed in the liver than the skin, *cyp3a80*, was recently reported as a colour candidate for red morph in *R. sirensis* (Twomey, Johnson, et al., 2020; Twomey, Kain, et al., 2020). Similarly, in other ectotherms like fishes and reptiles, yellow and orange colorations are associated with the expression of genes of these two pigment classes (Andrade & Carneiro, 2021; McLean et al., 2019; Sefc et al., 2014). The predominance of xanthophores in the skin of orange *B. actaeus* morphs and the absence of DEGs linked to carotenoids and pteridines synthesis were unexpected. One possible explanation for this discrepancy is that carotenoid-related genes might be rather expressed in the liver, as shown in *R. sirensis* (Twomey, Johnson, et al., 2020; Twomey, Kain, et al., 2020). Alternatively, most of these genes might have been expressed during development (Stuckert et al., 2023), with some basal expression levels in the adults that we could not detect.

#### 4.4.3 | Other genes associated with pigmentation

Additional colour-related genes were identified in our dataset, but the involvement in colour differentiation needs to be clarified. Among these DEGs, the grey versus orange morph has two genes up-regulated (*fanci*, *mcm2*); the orange versus all morphs has one gene down-regulated (*inpp5b*) and the green versus grey morph has one gene up-regulated (*sdca4*). They all have putative structural functions that might be in DNA repair or replication and encoding several functions influencing the cell cycle (Baxter et al., 2019; Ooms et al., 2009). *fanci* was linked with hyperpigmentation or spots in human skin, *mcm2* influences hair greying with age in mice and *sdca4* might be related to melanin abnormalities (Baxter et al., 2019).

#### 4.4.4 | Transcriptome-wide association analysis between gene expression and predator perceptual space

The results of the association analyses highlighted the contribution of melanin-related genes *oca2*, *dct*, *mlana*, *slc24a5* and *tyrp1* to colour variation in *B. actaeus* individuals. All these genes show decreased expression associated with higher values in the x-coordinate axis of predator perception (red-orange hues) (Table 3). An additional set of 13 genes was also found to be associated with colour variation in our results but have not been related to colour variation in the literature. Of these, *bmp2*, *c7h10orf95*, *lca5*, *ppp1r3c.2*, *sik1*, *klhdc7b*, *yipf7* and a paralogue of *jun* decrease their expression as the skin colour changes to more orange, while the other five genes (*derl3*, *jmjd7*,



LOC116412396, *znf574* and a *cdhr3* paralogue) increase in expression (Figure S8). These genes constitute interesting candidates for future studies, necessary to understand the molecular mechanisms responsible for colour variation in frogs.

## 4.5 | General perspectives

By employing an integrative approach, our study has raised intriguing questions on colour variation in a non-model organism, *B. actaeus*. Our bird visual modelling consistently indicates that visually oriented observers perceive colour variation among *B. actaeus* morphs differently. Also, our findings revealing the absence of iridophores in the skin of *B. actaeus* morphs may appear to contradict previous findings used to explain how green colour arises from the interaction of three chromatophores: xanthophores, iridophores and melanophores (Bagnara & Matsumoto, 2006). Further, our transcriptomic analysis of skin identified DEGs primarily linked to melanin synthesis, underscoring their role in colour polytypism.

Notably, many of the identified genes actively participate in the typical pigmentation pathways observed in vertebrates. This correlation between divergent genetic profiles (gene expression) and convergent analogous colour phenotypes or patterns supports the idea of genetic constraints existing across species. However, it also underscores the inherent flexibility of adaptive mechanisms in colour production. For example, among the species of the genus *Ranitomeya*, similar colour phenotypes can be explained by parallel and non-parallel convergence related to carotenoid and pterin pigments (Twomey et al., 2023). Similarly, studies in other vertebrates have shown that intra-population divergence produces similar phenotypes despite variations in colour-related genes and/or functional mechanisms within those genes (Henning et al., 2010; Hubbard et al., 2010; Manceau et al., 2010; Nilsson-Sköld et al., 2016).

We emphasize the need for further research in the *Brachycephalus* system to gain insights into the mechanisms underlying colour polytypism, given its distinct biology compared to dendrobatids. Future studies should: (1) identify predators potentially sensitive to UV through visual models and in situ experiments; (2) assess the chemical defence; (3) compare toxicity levels among morphs; (4) investigate colour's potential role in predator avoidance and sexual selection; (5) elucidate the observed green colour derived of skin structures containing xanthophores and melanophores; (6) characterize skin pigments through biochemical identification to clarify expression patterns of the *cbs* gene and assess potential masking effects of melanin on other pigments and (7) analyse differential expression in organs involved in pigment uptake and metabolism.

## 5 | CONCLUSIONS

In this study, we addressed the phenotypic variation and the genetic basis for the colour polytypism in *B. actaeus*. Through bird visual modelling, we classified colour morphs and explored their potential

functions. We identified pigment cells in toadlet skin corresponding to colour and structure. We recognized various candidate colour-related genes differentially expressed among this species' brown, grey, green and orange morphs. Most of these genes are strongly associated with melanin production, highlighting their importance in colour variation, aligning with variation in melanophores abundance among morphs. These findings provide the first molecular explanation for amphibian colour variation beyond poison frogs and salamanders, integrating molecular data with structural information. Our study underscores the importance of investigating polymorphic species across other groups to gain a comprehensive understanding of the diverse pathways that contribute to the evolution of pigment production in amphibian skin. Future studies should integrate behaviour, ecology and phylogenetic relationships to elucidate the evolutionary process driving adaptive coloration and its potential impact on reproductive isolation. Given this, polytypic species offer valuable insights into fundamental biological processes, including, but not limited to, local adaptation, the persistence of genetic diversity and speciation. Conservation efforts are crucial to preserving the evolutionary history of each species' colour morph.

## AUTHOR CONTRIBUTIONS

Conceptualization: J.P.C.M., H.P., M.L.L., A.E.B., C.F.B.H., A.R. Conducting the fieldwork: J.P.C.M., M.L.L., A.E.B., E.C.N. Performing research: J.P.C.M., H.P., M.L.L., A.E.B., C.F.B.H., A.R. Conducting bioinformatic analyses: J.P.C.M., A.R. Analysing data: J.P.C.M., H.P., M.L.L., A.E.B., A.R. Drafting of the manuscript: J.P.C.M., H.P., M.L.L., A.E.B., A.R. Review and editing of the manuscript: J.P.C.M., H.P., M.L.L., A.E.B., C.F.B.H., E.C.N., T.H.C., A.R. All authors read, reviewed and approved the final manuscript.

## ACKNOWLEDGEMENTS

We thank Patricia Maltempi and Marcelo Silva in Brazil and Felix Felmy and Alina Zacher in Hannover for the helpful access to photomicroscopes. We are grateful to Ariadne Sabbag for her invaluable help with TEM images. We also thank A. Sabbag, Carla Lopes, Evan Twomey, Marcus Thadeu T. Santos, Mariana Vasconcellos, P. Maltempi and Taran Grant for their comments on the previous version of the manuscript. Computations were performed at the Zentrale Informations- und Datenverarbeitungsservice der Stiftung TiHo Hannover (TiHo-IDS) and were kindly facilitated by Silvester Jordan and Frank Burkhart. J.P.C.M. thanks the Institute of Zoology of TiHo Hannover for its support. Open Access funding enabled and organized by Projekt DEAL.

## FUNDING INFORMATION

This work was supported by grants from the São Paulo Research Foundation to J.P.C.M. (FAPESP #2018/09691-0 and #2021/08744-9) and C.F.B.H. (FAPESP#2021/10639-5). The work of C.F.B.H. and M.L.L. was also funded by The National Council for Scientific and Technological Development (CNPq #306623/2018; CNPq-PDS #163546/2020-7). The work of A.E.B. was funded by the Agencia Nacional de Promoción Científica y Tecnológica (PICT #2020/2939)

and Consejo Nacional de Investigaciones Científicas y Técnicas (CONICET #PIP/2021-2023). Sequencing costs were covered by a Deutsche Forschungsgemeinschaft (DFG) research grant to A.R. (RO5508/2-1), a Deutsche Gesellschaft für Herpetologie und Terrarienkunde (DGHT) grant to H.P. and J.P.C.M. (WP-01/2022) and FAPESP (#2021/08744-9).

## CONFLICT OF INTEREST STATEMENT

The authors declare no conflicts of interest.

## OPEN RESEARCH BADGES



This article has earned an Open Data badge for making publicly available the digitally-shareable data necessary to reproduce the reported results. The data is available at <https://www.ebi.ac.uk/ena/browser/view/PRJNA1112388>.

## DATA AVAILABILITY STATEMENT

RNA-Seq reads have been deposited in the NCBI Sequence Read Archive (SRA), under the BioProject accession number PRJNA1112388. Code for assemblies, annotation and all subsequent analyses are all available on GitHub ([https://github.com/ArielRodrig/Brachycephalus\\_RNASeq](https://github.com/ArielRodrig/Brachycephalus_RNASeq)).

## BENEFIT-SHARING STATEMENT

This research project is a collaborative effort between Brazilian, German, Argentinian and Cuban scientists, building upon the initiative of the Brazilian scientific community. The outcomes of this study will be disseminated to the relevant authorities tasked with implementing conservation measures for the species under consideration.

## ORCID

Juliane P. C. Monteiro <https://orcid.org/0000-0002-1172-4560>

Heike Pröhl <https://orcid.org/0000-0003-4918-5838>

Mariana L. Lyra <https://orcid.org/0000-0002-7863-4965>

Andrés E. Brunetti <https://orcid.org/0000-0001-7974-6099>

Eli C. de Nardin <https://orcid.org/0009-0009-7602-4504>

Thais H. Condez <https://orcid.org/0000-0003-0736-4651>

Célio F. B. Haddad <https://orcid.org/0000-0003-1057-5660>

Ariel Rodríguez <https://orcid.org/0000-0003-1936-793X>

## REFERENCES

- Alexander, D. H., Novembre, J., & Lange, K. (2009). Fast model-based estimation of ancestry in unrelated individuals. *Genome Research*, 19(9), 1655–1664. <https://doi.org/10.1101/gr.094052.109>
- Amann, P. M., Luo, C., Owen, R. W., Hofmann, C., Freudenberger, M., Schadendorf, D., Eichmüller, S. B., & Bazhin, A. V. (2012). Vitamin A metabolism in benign and malignant melanocytic skin cells: Importance of lecithin/retinol acyltransferase and RPE65. *Journal of Cellular Physiology*, 227(2), 718–728. <https://doi.org/10.1002/jcp.22779>
- Andrade, P., & Carneiro, M. (2021). Pterin-based pigmentation in animals. *Biology Letters*, 17, 20210221. <https://doi.org/10.1098/rsbl.2021.0221>
- Andrade, P., Lyra, M. L., Zina, J., Bastos, D. F. O., Brunetti, A. E., Baêta, D., Afonso, S., Brunes, T. O., Taucce, P. P. G., Carneiro, M., Haddad, C. F. B., & Sequeira, F. (2022). Draft genome and multi-tissue transcriptome assemblies of the Neotropical leaf-frog *Phyllomedusa bahiana*. *G3: Genes, Genomes, Genetics*, 12(12), jkac270. <https://doi.org/10.1093/g3journal/jkac270>
- Andrews, S. (2010). FastQC: A quality control tool for high throughput sequence data. <http://www.bioinformatics.babraham.ac.uk/projects/fastqc/>
- Arganda-Carreras, I., Kaynig, V., Rueden, C., Eliceiri, K. W., Schindelin, J., Cardona, A., & Sebastian Seung, H. (2017). Trainable Weka Segmentation: A machine learning tool for microscopy pixel classification. *Bioinformatics*, 33(15), 2424–2426. <https://doi.org/10.1093/bioinformatics/btx180>
- Bagnara, J. T., Fernandez, P. J., & Fujii, R. (2007). On the blue coloration of vertebrates. *Pigment Cell Research*, 20(1), 14–26. <https://doi.org/10.1111/j.1600-0749.2006.00360.x>
- Bagnara, J. T., & Hadley, M. E. (1969). The control of bright colored pigment cells of fishes and amphibians. *American Zoologist*, 9, 465–478.
- Bagnara, J. T., & Matsumoto, J. (2006). Comparative anatomy and physiology of pigment cells in nonmammalian tissues. In J. J. Nordlund, R. E. Boissy, V. J. Hearing, R. A. King, W. S. Oetting, & J.-P. Ortonne (Eds.), *The pigmentary system: Physiology and pathophysiology* (2nd ed.). Blackwell Publishing Ltd. <https://doi.org/10.1002/9780470987100>
- Bagnara, J. T., Taylor, J. D., & Hadley, M. E. (1968). The dermal chromatophore unit. *The Journal of Cell Biology*, 38, 67–79.
- Baxter, L. L., Watkins-Chow, D. E., Pavan, W. J., & Loftus, S. K. (2019). A curated gene list for expanding the horizons of pigmentation biology. *Pigment Cell and Melanoma Research*, 32(3), 348–358. <https://doi.org/10.1111/pcmr.12743>
- Bolger, A. M., Lohse, M., & Usadel, B. (2014). Trimmomatic: A flexible trimmer for Illumina sequence data. *Bioinformatics*, 30(15), 2114–2120. <https://doi.org/10.1093/bioinformatics/btu170>
- Braasch, I., & Scharl, M. (2014). Evolution of endothelin receptors in vertebrates. *General and Comparative Endocrinology*, 209, 21–34. <https://doi.org/10.1016/j.ygcen.2014.06.028>
- Braasch, I., Scharl, M., & Volff, J. N. (2007). Evolution of pigment synthesis pathways by gene and genome duplication in fish. *BMC Evolutionary Biology*, 7, 74. <https://doi.org/10.1186/1471-2148-7-74>
- Bray, N. L., Pimentel, H., Melsted, P., & Pachter, L. (2016). Near-optimal probabilistic RNA-seq quantification. *Nature Biotechnology*, 34(5), 525–527. <https://doi.org/10.1038/nbt.3519>
- Briolat, E. S., Burdfield-Steel, E. R., Paul, S. C., Rönkä, K. H., Seymoure, B. M., Stankowich, T., & Stuckert, A. M. M. (2019). Diversity in warning coloration: Selective paradox or the norm? *Biological Reviews*, 94(2), 388–414. <https://doi.org/10.1111/brv.12460>
- Brunetti, A. E., Hermida, G. N., Iurman, M. G., & Faivovich, J. (2016). Odorous secretions in anurans: Morphological and functional assessment of serous glands as a source of volatile compounds in the skin of the treefrog *Hypsiboas pulchellus* (Amphibia: Anura: Hylidae). *Journal of Anatomy*, 228(3), 430–442. <https://doi.org/10.1111/joa.12413>
- Brusa, O., Bellati, A., Meuche, I., Mundy, N. I., & Pröhl, H. (2013). Divergent evolution in the polymorphic granular poison-dart frog, *Oophaga granulifera*: Genetics, coloration, advertisement calls and morphology. *Journal of Biogeography*, 40(2), 394–408. <https://doi.org/10.1111/j.1365-2699.2012.02786.x>
- Buchfink, B., Xie, C., & Huson, D. H. (2014). Fast and sensitive protein alignment using DIAMOND. *Nature Methods*, 12(1), 59–60. <https://doi.org/10.1038/nmeth.3176>
- Burgon, J. D., Vieites, D. R., Jacobs, A., Weidt, S. K., Gunter, H. M., Steinfartz, S., Burgess, K., Mable, B. K., & Elmer, K. R. (2020). Functional colour genes and signals of selection in colour-polymorphic salamanders.

- Molecular Ecology*, 29(7), 1284–1299. <https://doi.org/10.1111/mec.15411>
- Bushmanova, E., Antipov, D., Lapidus, A., & Prijbelski, A. D. (2019). RnaSPAdes: A de novo transcriptome assembler and its application to RNA-Seq data. *GigaScience*, 8(9), giz100. <https://doi.org/10.1093/gigascience/giz100>
- Bushnell, B. (2014). *BBtools*. <https://sourceforge.net/projects/bbmap/>
- Caro, T. (2017). Wallace on coloration: Contemporary perspective and unresolved insights. *Trends in Ecology & Evolution*, 32(1), 23–30. <https://doi.org/10.1016/j.tree.2016.10.003>
- Caro, T., & Ruxton, G. (2019). Aposematism: Unpacking the defences. *Trends in Ecology & Evolution*, 34(7), 595–604. <https://doi.org/10.1016/j.tree.2019.02.015>
- Carreira, S., Goodall, J., Aksan, I., La Rocca, S. A., Galibert, M.-D., Denat, L., Larue, L., & Goding, C. R. (2005). Mitf cooperates with Rb1 and activates p21<sup>Cip1</sup> expression to regulate cycle cell progression. *Nature*, 433(17), 764–769.
- Carvalho, A. L. (1940). Observações sobre casos de batracofagia entre as aves. *Memórias do Instituto Oswaldo Cruz*, 35(3), 575–576.
- Casas-Cardona, S., Márquez, R., & Vargas-Salinas, F. (2018). Different colour morphs of the poison frog *Andinobates bombetes* (Dendrobatidae) are similarly effective visual predator deterrents. *Ethology*, 124(4), 245–255. <https://doi.org/10.1111/eth.12729>
- Chimetto Tonon, L. A., Rua, C., Crnkovic, C. M., Bernardi, D. I., Pires Junior, O. R., Haddad, C. F. B., Pedrosa, C. S. G., Souza, L. R. Q., Rehen, S. K., de Azevedo, G. P. R., Thompson, C. C., Thompson, F. L., & Berlinck, R. G. S. (2021). Microbiome associated with the tetrodotoxin-bearing anuran *Brachycephalus pitanga*. *Toxicon*, 203, 139–146. <https://doi.org/10.1016/j.toxicon.2021.10.002>
- Chouteau, M., & Angers, B. (2012). Wright's shifting balance theory and the diversification of aposematic signals. *PLoS One*, 7(3), e34028. <https://doi.org/10.1371/journal.pone.0034028>
- Cieslak, M., Reissmann, M., Hofreiter, M., & Ludwig, A. (2011). Colours of domestication. *Biological Reviews*, 86(4), 885–899. <https://doi.org/10.1111/j.1469-185x.2011.00177.x>
- Condez, T. H., Haddad, C. F. B., & Zamudio, K. R. (2020). Historical biogeography and multi-trait evolution in miniature toadlets of the genus *Brachycephalus* (Anura: Brachycephalidae). *Biological Journal of the Linnean Society*, 129(3), 664–686. <https://doi.org/10.1093/biolinean/blz200>
- Crothers, L., Gering, E., & Cummings, M. (2011). Aposematic signal variation predicts male-male interactions in a polymorphic poison frog. *Evolution*, 65(2), 599–605.
- Danecek, P., Auton, A., Abecasis, G., Albers, C. A., Banks, E., DePristo, M. A., Handsaker, R. E., Lunter, G., Marth, G. T., Sherry, S. T., McVean, G., & Durbin, R. (2011). The variant call format and VCFtools. *Bioinformatics*, 27(15), 2156–2158. <https://doi.org/10.1093/bioinformatics/btr330>
- Davidson, N. M., Hawkins, A. D. K., & Oshlack, A. (2017). SuperTranscripts: A data driven reference for analysis and visualisation of transcriptomes. *Genome Biology*, 18(1), 148. <https://doi.org/10.1186/s13059-017-1284-1>
- Davidson, N. M., & Oshlack, A. (2014). Corset: Enabling differential gene expression analysis for de novo assembled transcriptomes. *Genome Biology*, 15, 410. <https://doi.org/10.1186/s13059-014-0410-6>
- Dobin, A., Davis, C. A., Schlesinger, F., Drenkow, J., Zaleski, C., Jha, S., Batut, P., Chaisson, M., & Gingeras, T. R. (2013). STAR: Ultrafast universal RNA-seq aligner. *Bioinformatics*, 29(1), 15–21. <https://doi.org/10.1093/bioinformatics/bts635>
- dos Reis, S. F., Clemente-Carvalho, R. B. G., dos Santos, C. M. S. F. F., Lopes, R. T., Von Zuben, F. J., Laborda, P. R., & Perez, S. I. (2020). Skull diversity and evolution in miniaturized amphibians, genus *Brachycephalus* (Anura: Brachycephalidae). *Anatomical Record*, 304(6), 1329–1343. <https://doi.org/10.1002/ar.24554>
- Dreher, C. E., Cummings, M. E., & Pröhl, H. (2015). An analysis of predator selection to affect aposematic coloration in a poison frog species. *PLoS One*, 10(6), e0130571. <https://doi.org/10.1371/journal.pone.0130571>
- Emberts, Z., & Wiens, J. J. (2022). Why are animals conspicuously colored? Evolution of sexual versus warning signals in land vertebrates. *Evolution*, 76(12), 2879–2892. <https://doi.org/10.1111/evo.14636>
- Fang, W., Huang, J., Li, S., & Lu, J. (2022). Identification of pigment genes (melanin, carotenoid and pteridine) associated with skin color variant in red tilapia using transcriptome analysis. *Aquaculture*, 547, 737429. <https://doi.org/10.1016/j.aquaculture.2021.737429>
- Fisher, M., James-Zorn, C., Ponferrada, V., Bell, A. J., Sundararaj, N., Segerdell, E., Chaturvedi, P., Bayyari, N., Chu, S., Pells, T., Lotay, V., Agalakov, S., Wang, D. Z., Arshinoff, B. I., Foley, S., Karimi, K., Vize, P. D., & Zorn, A. M. (2023). Xenbase: Key features and resources of the *Xenopus* model organism knowledgebase. *Genetics*, 224(1), 1–13. <https://doi.org/10.1093/genetics/iyad018>
- Fraley, C., Raftery, A. E., & Murphy, T. B. (2012). *mclust version 4 for R: Normal mixture modeling for model-based clustering, classification, and density estimation*. <http://cran.r-project.org/web/packages/mclust/index.html>
- Frost, D. R. (2024). Amphibian species of the world: An online reference. Version 6.2 (accessed on 08 May 2024). Electronic Database available at <https://amphibiansoftheworld.amnh.org/index.php>. American Museum of Natural History, New York, USA. <https://doi.org/10.5531/db.vz.0001>
- Frost, S. K., & Robinson, S. J. (1984). Pigment cell differentiation in the fire-bellied toad, *Bombina orientalis*. I. Structural, chemical, and physical aspects of the adult pigment pattern. *Journal of Morphology*, 179, 229–242.
- Gilbert, D. G. (2019). Longest protein, longest transcript or most expression, for accurate gene reconstruction of transcriptomes? *BioRxiv*, 1–27. <https://doi.org/10.1101/829184>
- Goutte, S., Hariyani, I., Utzinger, K. D., Bourgeois, Y., & Boissinot, S. (2022). Genomic analyses reveal association of ASIP with a recurrently evolving adaptive color pattern in frogs. *Molecular Biology and Evolution*, 39(11), msac235. <https://doi.org/10.1093/molbev/msac235>
- Guo, W., Tzioutziou, N. A., Stephen, G., Milne, I., Calixto, C. P. G., Waugh, R., Brown, J. W. S., & Zhang, R. (2021). 3D RNA-seq: A powerful and flexible tool for rapid and accurate differential expression and alternative splicing analysis of RNA-seq data for biologists. *RNA Biology*, 18(11), 1574–1587. <https://doi.org/10.1080/15476286.2020.1858253>
- Haas, B. J., Papanicolaou, A., Yassour, M., Grabherr, M., Blood, P. D., Bowden, J., Couger, M. B., Eccles, D., Li, B., Lieber, M., Macmanes, M. D., Ott, M., Orvis, J., Pochet, N., Strozzi, F., Weeks, N., Westerman, R., William, T., Dewey, C. N., ... Regav, A. (2013). De novo transcript sequence reconstruction from RNA-seq using the trinity platform for reference generation and analysis. *Nature Protocols*, 8(8), 1494–1512. <https://doi.org/10.1038/nprot.2013.084>
- Hanifin, C. T. (2010). The chemical and evolutionary ecology of tetrodotoxin (TTX) toxicity in terrestrial vertebrates. *Marine Drugs*, 8(3), 577–593. <https://doi.org/10.3390/md8030577>
- Hart, A. J., Ginzburg, S., Xu, M., Fisher, C. R., Rahmatpour, N., Mitton, J. B., Paul, R., & Wegrzyn, J. L. (2020). EnTAP: Bringing faster and smarter functional annotation to non-model eukaryotic transcriptomes. *Molecular Ecology Resources*, 20(2), 591–604. <https://doi.org/10.1111/1755-0998.13106>
- Hashimoto, H., Godo, M., Futahashi, R., Kelsh, R., & Akiyama, T. (2021). Pigments, pigment cells and pigment patterns. In H. Hashimoto, M. Goda, R. Futahashi, R. Kelsh, & T. Akiyama (Eds.), *Pigments, pigment cells and pigment patterns* (1st ed.). Springer International Publishing. <https://doi.org/10.1007/978-981-16-1490-3>
- Henning, F., Jones, J. C., Franchini, P., & Meyer, A. (2013). Transcriptomics of morphological color change in polychromatic Midas cichlids. *BMC Genomics*, 14(1), 1–13. <https://doi.org/10.1186/1471-2164-14-171>

- Henning, F., Renz, A. J., Fukamachi, S., & Meyer, A. (2010). Genetic, comparative genomic, and expression analyses of the Mc1r locus in the polychromatic Midas cichlid fish (Teleostei, Cichlidae *Amphilophus* sp.) species group. *Journal of Molecular Evolution*, 70(5), 405–412. <https://doi.org/10.1007/s00239-010-9340-4>
- Higdon, C. W., Mitra, R. D., & Johnson, S. L. (2013). Gene expression analysis of zebrafish melanocytes, iridophores, and retinal pigmented epithelium reveals indicators of biological function and developmental origin. *PLoS One*, 8(7), e67801. <https://doi.org/10.1371/journal.pone.0067801>
- Hoashi, T., Watabe, H., Muller, J., Yamaguchi, Y., Vieira, W. D., & Hearing, V. J. (2005). MART-1 is required for the function of the melanosomal matrix protein PMEL17/GP100 and the maturation of melanosomes. *Journal of Biological Chemistry*, 280(14), 14006–14016. <https://doi.org/10.1074/jbc.M413692200>
- Hoekstra, H. E. (2006). Genetics, development and evolution of adaptive pigmentation in vertebrates. *Heredity*, 97(3), 222–234. <https://doi.org/10.1038/sj.hdy.6800861>
- Hofreiter, M., & Schöneberg, T. (2010). The genetic and evolutionary basis of colour variation in vertebrates. *Cellular and Molecular Life Sciences*, 67(15), 2591–2603. <https://doi.org/10.1007/s00018-010-0333-7>
- Hubbard, J. K., Uy, J. A. C., Hauber, M. E., Hoekstra, H. E., & Safran, R. J. (2010). Vertebrate pigmentation: From underlying genes to adaptive function. *Trends in Genetics*, 26(5), 231–239. <https://doi.org/10.1016/j.tig.2010.02.002>
- Huerta-Cepas, J., Szklarczyk, D., Heller, D., Hernández-Plaza, A., Forslund, S. K., Cook, H., Mende, D. R., Letunic, I., Rattei, T., Jensen, L. J., Von Mering, C., & Bork, P. (2019). EggNOG 5.0: A hierarchical, functionally and phylogenetically annotated orthology resource based on 5090 organisms and 2502 viruses. *Nucleic Acids Research*, 47(D1), D309–D314. <https://doi.org/10.1093/nar/gky1085>
- Hutton, P., Seymoure, B. M., McGraw, K. J., Ligon, R. A., & Simpson, R. K. (2015). Dynamic color communication. *Current Opinion in Behavioral Sciences*, 6, 41–49. <https://doi.org/10.1016/j.cobeha.2015.08.007>
- Kindermann, C., & Hero, J. M. (2016). Pigment cell distribution in a rapid colour changing amphibian (*Litoria wilcoxii*). *Zoomorphology*, 135(2), 197–203. <https://doi.org/10.1007/s00435-016-0303-1>
- Kopylova, E., Noé, L., & Touzet, H. (2012). SortMeRNA: Fast and accurate filtering of ribosomal RNAs in metatranscriptomic data. *Bioinformatics*, 28(24), 3211–3217. <https://doi.org/10.1093/bioinformatics/bts611>
- Lamason, R. L., Mohideen, M.-A. P., Mest, J. R., Wong, A. C., Norton-Heather, L., Aros, M. C., Juryneć, M. J., Mao, X., Humphreville, V. R., Humbert, J. E., Sinha, S., Moore, J. L., Jagadeeswaran, P., Zhao, W., Ning, G., Makalowska, I., McKeigue, P. M., Kittles, R., Parra, E. J., ... Cheng, K. C. (2002). SLC24A5, a putative cation exchanger, affects pigmentation in zebrafish and humans. *Science*, 310, 1782–1786.
- Langfelder, P., & Horvath, S. (2008). WGCNA: An R package for weighted correlation network analysis. *BMC Bioinformatics*, 9, 559. <https://doi.org/10.1186/1471-2105-9-559>
- Lazic, S. E. (2008). Why we should use simpler models if the data allow this: Relevance for ANOVA designs in experimental biology. *BMC Physiology*, 8(16), 2–7. <https://doi.org/10.1186/1472-6793-8-16>
- Lehman, M. R., González-Santoro, M., & Richards-Zawacki, C. L. (2024). Little evidence for color- or size-based mating preferences by male strawberry poison frogs (*Oophaga pumilio*). *Behavioral Ecology and Sociobiology*, 78(2), 11. <https://doi.org/10.1007/s00265-024-03436-9>
- Loftus, S. K., Larson, D. M., Baxter, L. L., Antonellis, A., Chen, Y., Wu, X., Jiang, Y., Bittner, M., Hammer, J. A., III, & Pavan, W. J. (2002). Mutation of melanosome protein RAB38 in chocolate mice. *Proceedings of the National Academy of Sciences of the United States of America*, 99(7), 4471–4476.
- Lyra, M. L., Monteiro, J. P. C., Rancilhac, L., Irisarri, I., Sanchez, E., Condez, T. H., Rojas-Padilla, O., Solé, M., Haddad, C. F. B., Vences, M., Künzel, S., & Toledo, L. F. (2021). Initial phylotranscriptomic confirmation of homoplastic evolution of the conspicuous coloration and bufoniform morphology of pumpkin-toadlets in the genus *Brachycephalus*. *Toxins*, 13(11), 816. <https://doi.org/10.3390/toxin13110816>
- Maan, M. E., & Cummings, M. E. (2008). Female preferences for aposematic signal components in a polymorphic poison frog. *Evolution*, 62(9), 2334–2345.
- Maan, M. E., & Cummings, M. E. (2012). Poison frog colors are honest signals of toxicity, particularly for bird predators. *The American Naturalist*, 179(1), E1–E14. <https://doi.org/10.5061/dryad.t979dp85>
- Maia, R., Gruson, H., Endler, J. A., & White, T. E. (2019). Pavo 2: New tools for the spectral and spatial analysis of colour in R. *Methods in Ecology and Evolution*, 10(7), 1097–1107. <https://doi.org/10.1111/2041-210X.13174>
- Maître, J. L., & Heisenberg, C. P. (2013). Three functions of cadherins in cell adhesion. *Current Biology*, 23(14), 626–633. <https://doi.org/10.1016/j.cub.2013.06.019>
- Mallet, J., & Joron, M. (1999). Evolution of diversity in warning color and mimicry: Polymorphisms, shifting balance, and speciation. *Annual Review of Ecology and Systematics*, 30, 201–233.
- Manceau, M., Domingues, V. S., Linnen, C. R., Rosenblum, E. B., & Hoekstra, H. E. (2010). Convergence in pigmentation at multiple levels: Mutations, genes and function. *Philosophical Transactions of the Royal Society, B: Biological Sciences*, 365(1552), 2439–2450. <https://doi.org/10.1098/rstb.2010.0104>
- McKenna, A., Hanna, M., Banks, E., Sivachenko, A., Cibulskis, K., Kernysky, A., Garimella, K., Altshuler, D., Gabriel, S., Daly, M., & DePristo, M. A. (2010). The genome analysis toolkit: A MapReduce framework for analyzing next-generation DNA sequencing data. *Genome Research*, 20(9), 1297–1303. <https://doi.org/10.1101/gr.107524.110>
- McLean, C. A., Lutz, A., Rankin, K. J., Elliott, A., Moussalli, A., & Stuart-Fox, D. (2019). Red carotenoids and associated gene expression explain colour variation in frillneck lizards. *Proceedings of the Royal Society B: Biological Sciences*, 286, 20191172. <https://doi.org/10.1098/rspb.2019.1172>
- McLean, C. A., Lutz, A., Rankin, K. J., Stuart-Fox, D., & Moussalli, A. (2017). Revealing the biochemical and genetic basis of color variation in a polymorphic lizard. *Molecular Biology and Evolution*, 34(8), 1924–1935. <https://doi.org/10.1093/molbev/msx136>
- McNamara, M. E., Rossi, V., Slater, T. S., Rogers, C. S., Ducrest, A. L., Dubey, S., & Roulin, A. (2021). Decoding the evolution of melanin in vertebrates. *Trends in Ecology & Evolution*, 36(5), 430–443. <https://doi.org/10.1016/j.tree.2020.12.012>
- Megía-Palma, R., Jorge, A., & Reguera, S. (2018). Raman spectroscopy reveals the presence of both eumelanin and pheomelanin in the skin of lacertids. *Journal of Herpetology*, 52(1), 67–73. <https://doi.org/10.1670/16-140>
- Mills, M. G., & Patterson, L. B. (2009). Not just black and white: Pigment pattern development and evolution in vertebrates. *Seminars in Cell and Developmental Biology*, 20(1), 72–81. <https://doi.org/10.1016/j.semcdb.2008.11.012>
- Monteiro, J. P. C., Condez, T. H., Garcia, P. C. A., Comitti, E. J., Amaral, I. B., & Haddad, C. F. B. (2018). A new species of *Brachycephalus* (Anura, Brachycephalidae) from the coast of Santa Catarina State, Southern Atlantic Forest, Brazil. *Zootaxa*, 4407(4), 483–505. <https://doi.org/10.11646/zootaxa.4407.4.2>
- Müller, F. (1879). *Ituna* and *Thyridia*; a remarkable case of mimicry in butterflies. *Proceedings of the Royal Entomological Society of London*, xx–xxix.
- Ng, A., Uribe, R. A., Yieh, L., Nuckels, R., & Gross, J. M. (2009). Zebrafish mutations in *gart* and *paics* identify crucial roles for de novo purine synthesis in vertebrate pigmentation and ocular development. *Development*, 136(15), 2601–2611. <https://doi.org/10.1242/dev.038315>



- Nicolaï, M. P. J., D'Alba, L., Goldenberg, J., Gansemans, Y., Van Nieuwerburgh, F., Clusella-Trullas, S., & Shawkey, M. D. (2021). Untangling the structural and molecular mechanisms underlying colour and rapid colour change in a lizard, *Agama Atrata*. *Molecular Ecology*, 30(10), 2262–2284. <https://doi.org/10.1111/mec.15901>
- Nilsson-Sköld, H. N., Aspögren, S., Cheney, K. L., & Wallin, M. (2016). Fish chromatophores—from molecular motors to animal behavior. *International Review of Cell and Molecular Biology*, 321, 171–219. <https://doi.org/10.1016/bs.ircmb.2015.09.005>
- Ooms, L. M., Horan, K. A., Rahman, P., Seaton, G., Gurung, R., Kethesparan, D. S., & Mitchell, C. A. (2009). The role of the inositol polyphosphate 5-phosphatases in cellular function and human disease. *Biochemical Journal*, 419(1), 29–49. <https://doi.org/10.1042/BJ20081673>
- Osorio, D., & Vorobyev, M. (2008). A review of the evolution of animal colour vision and visual communication signals. *Vision Research*, 48(20), 2042–2051. <https://doi.org/10.1016/j.visres.2008.06.018>
- Palacios-Rodríguez, P., González-Santoro, M., Amézquita, A., & Brunetti, A. E. (2022). Sexual dichromatism in a cryptic poison frog is correlated with female tadpole transport. *Evolutionary Ecology*, 36(1), 153–162. <https://doi.org/10.1007/s10682-021-10147-4>
- Pie, M. R., Meyer, A. L. S., Firkowski, C. R., Ribeiro, L. F., & Bornschein, M. R. (2013). Understanding the mechanisms underlying the distribution of microendemic montane frogs (*Brachycephalus* spp., Terrarana: Brachycephalidae) in the Brazilian Atlantic Rainforest. *Ecological Modelling*, 250, 165–176. <https://doi.org/10.1016/j.ecolmodel.2012.10.019>
- Pie, M. R., Ribeiro, L. F., Confetti, A. E., Nadaline, M. J., & Bornschein, M. R. (2018). A new species of *Brachycephalus* (Anura: Brachycephalidae) from Southern Brazil. *PeerJ*, 6, e5683. <https://doi.org/10.7717/peerj.5683>
- Pike, T. W. (2012). Preserving perceptual distances in chromaticity diagrams. *Behavioral Ecology*, 23(4), 723–728. <https://doi.org/10.1093/beheco/ars018>
- Pires, O. R., Sebben, A., Schwartz, E. F., Morales, R. A. V., Bloch, C., & Schwartz, C. A. (2005). Further report of the occurrence of tetrodotoxin and new analogues in the anuran family Brachycephalidae. *Toxicon*, 45(1), 73–79. <https://doi.org/10.1016/j.toxicon.2004.09.016>
- Pombal, J. P., Jr., Sazima, I., & Haddad, C. F. B. (1994). Breeding behavior of the pumpkin toadlet, *Brachycephalus ephippium* (Brachycephalidae). *Journal of Herpetology*, 28(4), 516–519.
- Posso-Terranova, A., & Andrés, J. (2017). Diversification and convergence of aposematic phenotypes: Truncated receptors and cellular arrangements mediate rapid evolution of coloration in harlequin poison frogs. *Evolution*, 71(11), 2677–2692. <https://doi.org/10.1111/evo.13335>
- Pröhl, H., & Ostrowski, T. (2011). Behavioural elements reflect phenotypic colour divergence in a poison frog. *Evolutionary Ecology*, 25(5), 993–1015. <https://doi.org/10.1007/s10682-010-9455-5>
- Purcell, S., Neale, B., Todd-Brown, K., Thomas, L., Ferreira, M. A. R., Bender, D., Maller, J., Sklar, P., De Bakker, P. I. W., Daly, M. J., & Sham, P. C. (2007). PLINK: A tool set for whole-genome association and population-based linkage analyses. *American Journal of Human Genetics*, 81(3), 559–575. <https://doi.org/10.1086/519795>
- R Core Team. (2021). R: A language and environment for statistical computing. R Foundation for Statistical Computing. <https://www.R-project.org/>
- Rebouças, R., Carollo, A. B., de Freitas, M. O., Lambertini, C., Dos Santos, R. M. N., & Toledo, L. F. (2019). Is the conspicuous dorsal coloration of the Atlantic Forest pumpkin toadlets aposematic? *Salamandra*, 55(1), 39–47.
- Renoult, J. P., Kelber, A., & Schaefer, H. M. (2017). Colour spaces in ecology and evolutionary biology. *Biological Reviews*, 92(1), 292–315. <https://doi.org/10.1111/brv.12230>
- Reynolds, R. G., & Fitzpatrick, B. M. (2007). Assortative mating in poison-dart frogs based on an ecologically important trait. *Evolution*, 61(9), 2253–2259. <https://doi.org/10.1111/j.1558-5646.2007.00174.x>
- Ribeiro, L. F., Blackburn, D. C., Stanley, E. L., Pie, M. R., & Bornschein, M. R. (2017). Two new species of the *Brachycephalus pernix* group (Anura: Brachycephalidae) from the state of Paraná, southern Brazil. *PeerJ*, 5, e3603. <https://doi.org/10.7717/peerj.3603>
- Ritchie, M. E., Phipson, B., Wu, D., Hu, Y., Law, C. W., Shi, W., & Smyth, G. K. (2015). Limma powers differential expression analyses for RNA-sequencing and microarray studies. *Nucleic Acids Research*, 43(7), e47. <https://doi.org/10.1093/nar/gkv007>
- Rodríguez, A., Mundy, N. I., Ibáñez, R., & Pröhl, H. (2020). Being red, blue and green: The genetic basis of coloration differences in the strawberry poison frog (*Oophaga pumilio*). *BMC Genomics*, 21(1), 301. <https://doi.org/10.1186/s12864-020-6719-5>
- Rojas, B. (2017). Behavioural, ecological, and evolutionary aspects of diversity in frog colour patterns. *Biological Reviews*, 92(2), 1059–1080. <https://doi.org/10.1111/brv.12269>
- Rojas, B., Burdfield-Steel, E., De Pasqual, C., Gordon, S., Hernández, L., Mappes, J., Nokelainen, O., Rönkä, K., & Lindstedt, C. (2018). Multimodal aposematic signals and their emerging role in mate attraction. *Frontiers in Ecology and Evolution*, 6, 93. <https://doi.org/10.3389/fevo.2018.00093>
- Rojas, D., Lima, A. P., Momigliano, P., Simões, P. I., Dudaniec, R. Y., de Avila-Pires, T. C. S., Hoogmoed, M. S., da Cunha Bitar, Y. O., Kaefer, I. L., Amézquita, A., & Stow, A. (2020). The evolution of polymorphism in the warning coloration of the Amazonian poison frog *Adelphobates galactonotus*. *Heredity*, 124(3), 439–456. <https://doi.org/10.1038/s41437-019-0281-4>
- Rojas, B., Valkonen, J., & Nokelainen, O. (2015). Aposematism. *Current Biology*, 25(9), R350–R351. <https://doi.org/10.1016/j.cub.2015.02.015>
- Roland, A. B., Santos, J. C., Carriker, B. C., Caty, S. N., Tapia, E. E., Coloma, L. A., & O'Connell, L. A. (2017). Radiation of the polymorphic little devil poison frog (*Oophaga sylvatica*) in Ecuador. *Ecology and Evolution*, 7(22), 9750–9762. <https://doi.org/10.1002/ece3.3503>
- Ruxton, G. D., Allen, W. L., Sherratt, T. N., & Speed, M. P. (2018). *Avoiding attack: The evolutionary ecology of crypsis, aposematism, and mimicry* (2nd ed.). Oxford University Press.
- San-Jose, L. M., & Roulin, A. (2017). Genomics of coloration in natural animal populations. *Philosophical Transactions of the Royal Society, B: Biological Sciences*, 372, 20160337. <https://doi.org/10.1098/rstb.2016.0337>
- Schindelin, J., Arganda-Carreras, I., Frise, E., Kaynig, V., Longair, M., Pietzsch, T., Preibisch, S., Rueden, C., Saalfeld, S., Schmid, B., Tinevez, J. Y., White, D. J., Hartenstein, V., Eliceiri, K., Tomancak, P., & Cardona, A. (2012). Fiji: An open-source platform for biological-image analysis. *Nature Methods*, 9(7), 676–682. <https://doi.org/10.1038/nmeth.2019>
- Schneider, C. A., Rasband, W. S., & Eliceiri, K. W. (2012). NIH image to ImageJ: 25 years of image analysis HHS public access. *Nature Methods*, 9(7), 671–675.
- Sefc, K. M., Brown, A. C., & Clotfelter, E. D. (2014). Carotenoid-based coloration in cichlid fishes. *Comparative Biochemistry and Physiology - A Molecular and Integrative Physiology*, 173, 42–51. <https://doi.org/10.1016/j.cbpa.2014.03.006>
- Shawkey, M. D., & D'Alba, L. (2017). Interactions between colour-producing mechanisms and their effects on the integumentary colour palette. *Philosophical Transactions of the Royal Society, B: Biological Sciences*, 372, 20160536. <https://doi.org/10.1098/rstb.2016.0536>
- Simão, F. A., Waterhouse, R. M., Ioannidis, P., Kriventseva, E. V., & Zdobnov, E. M. (2015). BUSCO: Assessing genome assembly and annotation completeness with single-copy orthologs. *Bioinformatics*, 31(19), 3210–3212. <https://doi.org/10.1093/bioinformatics/btv351>

- Sofer, T., Kurniansyah, N., Aguet, F., Ardlie, K., Durda, P., Nickerson, D. A., Smith, J. D., Liu, Y., Gharib, S. A., Redline, S., Rich, S. S., Rotter, J. I., & Taylor, K. D. (2021). Benchmarking association analyses of continuous exposures with RNA-seq in observational studies. *Briefings in Bioinformatics*, 22(6), bbab194. <https://doi.org/10.1093/bib/bbab194>
- Stuart-Fox, D., Aulsebrook, A., Rankin, K. J., Dong, C. M., & McLean, C. A. (2021). Convergence and divergence in lizard colour polymorphisms. *Biological Reviews*, 96(1), 289–309. <https://doi.org/10.1111/brv.12656>
- Stuckert, A. M. M., Freeborn, L., Howell, K. A., Yang, Y., Nielsen, R., Richards-Zawacki, C., & MacManes, M. D. (2023). Transcriptomic analyses during development reveal mechanisms of integument structuring and color production. *Evolutionary Ecology*, 1–22. <https://doi.org/10.1007/s10682-023-10256-2>
- Stuckert, A. M. M., Moore, E., Coyle, K. P., Davison, I., MacManes, M. D., Roberts, R., & Summers, K. (2019). Variation in pigmentation gene expression is associated with distinct aposematic color morphs in the poison frog *Dendrobates auratus*. *BMC Evolutionary Biology*, 19, 85. <https://doi.org/10.1186/s12862-019-1410-7>
- Taboada, C., Brunetti, A. E., Lyra, M. L., Fitak, R. R., Soverna, A. F., Ron, S. R., Lagorio, M. G., Haddad, C. F. B., Lopes, N. P., Johnsen, S., Faivovich, J., Chemes, L. B., & Bari, S. E. (2020). Multiple origins of green coloration in frogs mediated by a novel biliverdin-binding serpin. *Proceedings of the National Academy of Sciences of the United States of America*, 117(31), 18574–18581. <https://doi.org/10.1073/pnas.2006771117>
- Thomas, P. D., Ebert, D., Muruganujan, A., Mushayahama, T., Albou, L. P., & Mi, H. (2022). PANTHER: Making genome-scale phylogenetics accessible to all. *Protein Science*, 31(1), 8–22. <https://doi.org/10.1002/pro.4218>
- Toledo, R. C., & Jared, C. (1993). The calcified dermal layer in anurans. *Comparative Biochemistry and Physiology*, 104(3), 443–448.
- Troschianko, J., & Stevens, M. (2015). Image calibration and analysis toolbox - a free software suite for objectively measuring reflectance, colour and pattern. *Methods in Ecology and Evolution*, 6(11), 1320–1331. <https://doi.org/10.1111/2041-210X.12439>
- Twomey, E., Johnson, J. D., Castroviejo-Fisher, S., & Van Bocxlaer, I. (2020). A ketocarotenoid-based colour polymorphism in the Sira poison frog *Ranitomeya sirensis* indicates novel gene interactions underlying aposematic signal variation. *Molecular Ecology*, 29(11), 2004–2015. <https://doi.org/10.1111/mec.15466>
- Twomey, E., Kain, M., Claeys, M., Summers, K., Castroviejo-Fisher, S., & Van Bocxlaer, I. (2020). Mechanisms for color convergence in a mimetic radiation of poison frogs. *American Naturalist*, 195(5), E132–E149. <https://doi.org/10.1086/708157>
- Twomey, E., Melo-Sampaio, P., Schulte, L. M., Bossuyt, F., Brown, J. L., & Castroviejo-Fisher, S. (2023). Multiple routes to color convergence in a radiation of Neotropical poison frogs. *Systematic Biology*, 72(6), 1247–1261. <https://doi.org/10.1093/sysbio/syad051>
- Vachtenheim, J., & Borovanský, J. (2010). "Transcription physiology" of pigment formation in melanocytes: Central role of MITF. *Experimental Dermatology*, 19(7), 617–627. <https://doi.org/10.1111/j.1600-0625.2009.01053.x>
- Van der Auwera, G. A., & O'Connor, B. D. (2020). Genomics in the cloud: using Docker. In *GATK, and WDL in Terra* (1st ed.). O'Reilly Media.
- van Rooij, J., Mandaviya, P. R., Claringbould, A., Felix, J. F., van Dongen, J., Jansen, R., Franke, L., BIOS Consortium, Hoen, P. A. C., Heijmans, B., & van Meurs, J. B. J. (2019). Evaluation of commonly used analysis strategies for epigenome- and transcriptome-wide association studies through replication of large-scale population studies. *Genome Biology*, 20(235), 235. <https://doi.org/10.1186/s13059-019-1878-x>
- VanBuren, C. A., & Everts, H. B. (2022). Vitamin A in skin and hair: An update. *Nutrients*, 14(2952), 2952. <https://doi.org/10.3390/nu14142952>
- Vorobyev, M., & Osorio, D. (1998). Receptor noise as a determinant of colour thresholds. *Proceedings of the Royal Society B: Biological Sciences*, 265, 351–358.
- Wan, Y. C., Méndez, M. J. N., O'Connell, L. A., Uricchio, L. H., Roland, A. B., Maan, M. E., Ron, S. R., Betancourt-Cundar, M., Pie, M. R., Howell, K. A., Richards-Zawacki, C. L., Cummings, M. E., Cannatella, D. C., Santos, J. C., & Tarvin, R. D. (2023). Selection on visual opsin genes in diurnal neotropical frogs and loss of the SWS2 opsin in poison frogs. *Molecular Biology and Evolution*, 40(10), msad206. <https://doi.org/10.1093/molbev/msad206>
- Wickham, H., Averick, M., Bryan, J., Chang, W., McGowan, L., François, R., Golemund, G., Hayes, A., Henry, L., Hester, J., Kuhn, M., Pedersen, T., Miller, E., Bache, S., Müller, K., Ooms, J., Robinson, D., Seidel, D., Spinu, V., ... Yutani, H. (2019). Welcome to the Tidyverse. *Journal of Open Source Software*, 4(43), 1686. <https://doi.org/10.21105/joss.01686>
- Willink, B., Brenes-Mora, E., Bolaños, F., & Pröhl, H. (2013). Not everything is black and white: Color and behavioral variation reveal a continuum between cryptic and aposematic strategies in a polymorphic poison frog. *Evolution*, 67(10), 2783–2794. <https://doi.org/10.1111/evo.12153>
- Willink, B., García-Rodríguez, A., Bolaños, F., & Pröhl, H. (2014). The interplay between multiple predators and prey colour divergence. *Biological Journal of the Linnean Society*, 113, 580–589.
- Wollenberg, K. C., Lötters, S., Mora-Ferrer, C., & Veith, M. (2008). Disentangling composite colour patterns in a poison frog species. *Biological Journal of the Linnean Society*, 93, 433–444.
- Wolnicka-Glubisz, A., Pecio, A., Podkowa, D., Kolodziejczyk, L. M., & Plonka, P. M. (2012). Pheomelanin in the skin of *Hymenochirus boettgeri* (Amphibia: Anura: Pipidae). *Experimental Dermatology*, 21(7), 537–540. <https://doi.org/10.1111/j.1600-0625.2012.01511.x>
- Wright, M. W., & Bowmaker, J. K. (2001). Retinal photoreceptors of paleognathous birds: The ostrich (*Struthio camelus*) and rhea (*Rhea americana*). *Vision Research*, 41, 1–12.
- Xie, Y., Wu, G., Tang, J., Luo, R., Patterson, J., Liu, S., Huang, W., He, G., Gu, S., Li, S., Zhou, X., Lam, T. W., Li, Y., Xu, X., Wong, G. K. S., & Wang, J. (2014). SOAPdenovo-trans: De novo transcriptome assembly with short RNA-Seq reads. *Bioinformatics*, 30(12), 1660–1666. <https://doi.org/10.1093/bioinformatics/btu077>
- Yeager, J., Derryberry, G. E., Blum, M. J., & Richards-Zawacki, C. L. (2023). Selection and admixture in a polytypic aposematic frog. *American Naturalist*, 201(2), 215–228. <https://doi.org/10.1086/722559>
- Yovanovich, C. A. M., Koskela, S. M., Nevala, N., Kondrashev, S. L., Kelber, A., & Donner, K. (2017). The dual rod system of amphibians supports colour discrimination at the absolute visual threshold. *Philosophical Transactions of the Royal Society, B: Biological Sciences*, 372(1717), 20160066. <https://doi.org/10.1098/rstb.2016.0066>
- Zhu, W., Wang, L., Dong, Z., Chen, X., Song, F., Liu, N., Yang, H., & Fu, J. (2016). Comparative transcriptome analysis identifies candidate genes related to skin color differentiation in red tilapia. *Scientific Reports*, 6, 31347. <https://doi.org/10.1038/srep31347>

## SUPPORTING INFORMATION

Additional supporting information can be found online in the Supporting Information section at the end of this article.

**How to cite this article:** Monteiro, J. P. C., Pröhl, H., Lyra, M. L., Brunetti, A. E., de Nardin, E. C., Condez, T. H., Haddad, C. F. B., & Rodríguez, A. (2024). Expression patterns of melanin-related genes are linked to crypsis and conspicuousness in a pumpkin toadlet. *Molecular Ecology*, 00, e17458. <https://doi.org/10.1111/mec.17458>